2017

Synthesis of Lanthanum chromite-Lanthanum manganite and LSCF-Lanthanum manganite core-shell particles via molten salt route

BOSTON UNIVERSITY

COLLEGE OF ENGINEERING

Thesis

SYNTHESIS OF LANTHANUM CHROMITE-LANTHANUM MANGANITE AND LSCF-LANTHANUM MANGANITE CORE-SHELL PARTICLES VIA MOLTEN SALT ROUTE

by

YUEXING ZHU

B.S., Donghua University, 2015

Submitted in partial fulfillment of the

requirements for the degree of

Master of Science

2017

Approved by

First Reader

Srikanth Gopalan, Ph.D.
Associate Professor of Mechanical Engineering
Associate Professor of Materials Science and Engineering

Second Reader

Emily M. Ryan, Ph.D.
Assistant Professor of Mechanical Engineering
Assistant Professor of Materials Science and Engineering

Third Reader

Michael A. Gevelber, Ph.D.
Associate Professor of Mechanical Engineering
Associate Professor of Materials Science and Engineering
Associate Professor of Systems Engineering

ACKNOWLEDGMENTS

I wish to sincerely thank my advisor, Professor Srikanth Gopalan, Associate Professor, Department of Mechanical Engineering, BU, for his supervision, inspiration, encouragement and support during my research. I also would like to express my greatest thanks to my thesis committee members: Professor Emily Ryan, Ph.D. and Professor Michael Gevelber, Ph.D. for their suggestions to my work.

The completion and success of my whole master studies and thesis would not have been possibly finished with the support of all my colleagues: Zhihao Sun, Yiwen Gong, Yanchen Lu, Scott Gillard, Ph.D., Ruofan Wang and Jane Banner. All of them helped me a lot when I was doing the experiments. They gave me plenty of valuable advice and discussions. I am also thankful to Dr. Jeff Bacon, Mr. Alexey Nikiforov and Ms. Anlee Krupp for guidance in XRD, SEM, EDS and STEM analysis during my research.

Moreover, I would like to thank my parents, Peishu Zhu and Huiping Zhang, for their selfless love and care along the way. They encouraged and mentored me patiently during every hard time I faced.

SYNTHESIS OF LANTHANUM CHROMITE-LANTHANUM MANGANITE AND LSCF-LANTHANUM MANGANITE CORE-SHELL PARTICLES VIA MOLTEN SALT ROUTE

YUEXING ZHU

ABSTRACT

Lanthanum chromite ($LaCrO_3$), Lanthanum manganite ($LaMnO_3$) and 40% strontium doped lanthanum cobalt iron oxide, $La_{0.6}Sr_{0.4}Co_{0.2}Fe_{0.8}O_3$ (LSCF-6428) are perovskite oxides which are widely used as interconnect or cathode materials in solid oxide fuel cells(SOFCs) due to their high electrical conductivity, good oxygen reduction kinetics, and good chemical stability. The solid state reaction route is the most commonly used method for synthesis of these materials. However, the solid state reaction method usually involves long-time mixing and high synthesis temperature (typically, >1200 ºC), which makes it time-consuming and costly. Molten salt synthesis, which occurs at much lower temperatures (350 ºC – 550 ºC) can offer better particle size and compositional control and reduced energy usage during materials synthesis.

In this study, $LaCrO_3$, $LaMnO_3$, and LSCF were synthesized in a molten salt eutectic of LiCl-KCl. A range of reaction temperature from 370 ºC to 600 ºC was investigated. It was found that a pure $LaMnO_3$ perovskite phase can be formed at as 400 ºC using the molten salt method and that LSCF powders were successfully synthesized at 500 ºC. When forming $LaCrO_3$ using the molten salt method, LaOCl was also formed at or above 400 ºC. The X-ray diffraction (XRD) results show this is an attractive alternative route of synthesis to decrease the reaction temperature. Both Scanning Electron

Microscopy (SEM) images and XRD patterns for $LaCrO_3$ showed that only cubic structures were formed at low temperature (400 ºC and 450 ºC) and then hexagonal structures started to appear at temperatures above 500 ºC.

The molten salt synthesis method was then used to prepare core-shell structures with $LaCrO_3$ or LSCF particles as the core and $LaMnO_3$ as the shell. Core-shell structures were characterized by Scanning Electron Microscopy (SEM), Scanning Transmission Electron Microscope (STEM) and Energy Dispersive X-ray Spectroscopy (EDS). It was found that the expected core-shell structures were successfully formed with the overall cubic structures.

Therefore, the molten salt synthesis method is a feasible method to decrease the operation temperature and form the core-shell structure.

TABLE OF CONTENTS

LIST OF TABLES

LIST OF FIGURES

LIST OF ABBREVIATIONS

Co_3O_4 ..... Cobalt (II, III) Oxide

Cr_2O_3 ..... Chromium Oxide

EDS ..... Energy Dispersive X-ray Spectroscopy

Fe_2O_3 ..... Iron (III) Oxide

KCl ..... Potassium Chloride

$LaCrO_3$ ..... Lanthanum Chromite

$LaMnO_3$ ..... Lanthanum Manganite

LaOCl ..... Lanthanum Oxychloride

$La_{0.6}Sr_{0.4}Co_{0.2}Fe_{0.8}O_3$ (LSCF) ..... 40% Strontium doped Lanthanum Cobalt Iron Oxide

La_2O_3 ..... Lanthanum Oxide

LiCl ..... Lithium Chloride

Mn_2O_3 ..... Manganese (III) Oxide

SEM ..... Scanning Electron Microscopy

$SrCO_3$ ..... Strontium Carbonate

STEM ..... Scanning Transmission Electron Microscopy

TEM ..... Transmission Electron Microscopy

XRD ..... X-ray Diffraction

1. INTRODUCTION

1.1. Solid Oxide Fuel Cells (SOFCs)

1.1.1. Introduction of SOFCs

Solid oxide fuel cells (SOFCs) are all solid-state energy conversion devices, which employ a solid oxide or ceramic electrolyte, cathode, and a ceramic metal composite anode. SOFCs have recently attracted great interest as efficient energy converting devices. They are environmentally friendly with minimum emissions and have high energy conversion efficiency with potentially low cost. SOFCs convert chemical energy from fuels directly to electricity and heat. The comparison of different types of fuel cells is shown in Table 1[1].

SOFCs have a simple structure with four components. They consist of an anode, and a cathode, which are separated and connected by a solid electrolyte. Each cell is connected to an adjacent cell by a bi-polar plate known as an interconnect. Interconnects are also used to separate fuel gas from air. $LaCrO_3$ and $LaMnO_3$ are the most common interconnect and cathode materials used in SOFC respectively.

Fuel cell type	Operating Temperature (ºC)	Power Generation Efficiency	Common Fuel	Common Electrolyte	Advantage	Disadvantage
SOFC (Solid Oxide Fuel Cell)	750–1000	45–65%	$CH_4/CO_2/H_2$	Yttria stabilized zirconia	•High efficiency •Fuel and catalysts flexibility •Solid electrolyte will not crack •Suitable for CHP	•High-T corrosion and breakdown of cell component •Long start-up time •Limited number of shutdowns
PEMFC (Polymer Electrolyte Membrane Fuel Cell)	60–120	30–60%	H_2/CO_2	polymer electrolyte	•Operate at a low temperature •Quick start-up	•fuels must be purified •expensive platinum catalyst is used •costs raising for polymer electrolyte
MCFC (Molten Carbonate Fuel Cell)	600–700	45–50%	$CH_4/CO_2/H_2$	Molten lithium, sodium or potassium carbonates soak in matrix	•High efficiency •Fuel flexibility •Suitable for CHP Hybrid/gas turbine cycle	•High temperature corrosion and breakdown of cell components •Long start-up time •Low power density
PAFC (Phosphoric Acid Fuel Cell)	180–200	35–42%	H_2/CO_2	Phosphoric acid soaked in matrix or imbibed in a membrane	•Suitable for CHP •Increased tolerance to fuel impurities	•Expensive catalysts •Long start-up time •Sulfur sensitivity •expensive platinum catalyst
PEFC (polymer electrolyte fuel cell)	25–90	35–40%	H_2/CO_2	Perfluorosulfonic acid	•reduces corrosion and electrolyte management problems •Low temperature •Quick start-up	•Expensive catalysts •Sensitive to fuel impurities
AFC (Alkaline Fuel Cell)	60–100	40–50%	H_2	Aqueous potassium hydroxide(KOH) soaked in membrane	•Wider range of stable materials for components •Low temperature •Quick start-up	•Sensitive to CO_2 in fuel and air •Electrolyte management (aqueous)

Table 1. Comparison of different fuel cells [1]

1.1.2. Perovskite structure

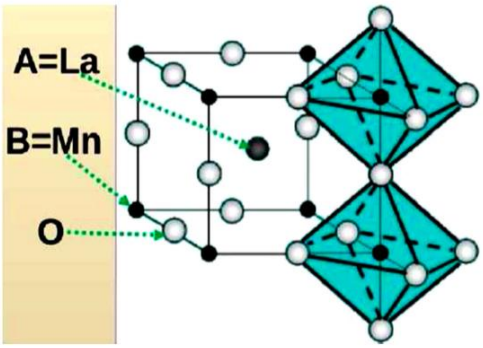

Fig. 1. cubic structure of $LaMnO_3$ perovskite [2]

$LaCrO_3$, $LaMnO_3$ and LSCF are all perovskite structure oxides in the ABO_3 family. The cubic perovskite structure exemplified by $LaMnO_3$ is shown in Fig.1. A Lanthanum (La) cation stands in the body center of its crystal unit. Manganese(Mn) cations occupy the eight corners of the cell and Oxygen(O) ions are in the middle of two Mn cations on the edges of the unit, which provides an ideal cell body centered cubic(BCC) structure.

1.2. Core-Shell particles

The broad definition of core-shell particles can be described as an inner core surrounded by an outer layer of shell. Core-shell structure particles have many technological applications in catalysis, biology, medicine, optical, electronic and magnetic devices [3–5]. Promising properties are not obtainable in the core or the shell materials alone, but appear when they are structured in a core-shell arrangement. In the field of SOFCs, core-shell particles have applications as cathode and anode materials. Specifically, a thin shell which shows a high level of oxygen surface area coverage but poor oxygen chemical diffusivity, can be combined with a core material that shows a high level of mixed ionic

and electronic conductivity (MIEC) with high oxygen chemical diffusivity. It results in a very high-performance cathode that shows high rates of oxygen reduction and transport.

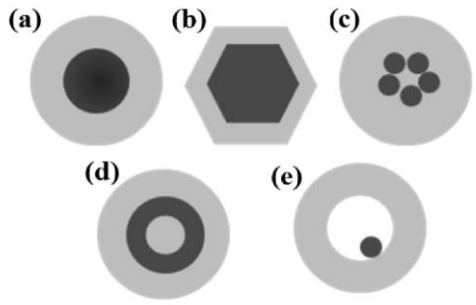

Fig. 2. Schematic shapes of core-shell particles [4]

Different shapes and composite materials are being studied. In Fig.2, different potential core-shell shapes are shown. They can be spherical, hexagonal or hollow structures and can consist of a wide range of combinations of inorganic and organic materials. Most importantly, they can be synthesized using inexpensive precursors. Core-shell particles can be produced by either a stepwise or a one-pot method based on different shell properties we need [3–5].

1.3. Solid State reaction

Solid state reaction is the most common way to synthesize $LaCrO_3$, $LaMnO_3$ and LSCF with all solid state chemical reactants. In this method, stoichiometric mixtures of oxide and/or carbonate precursors are heated to 1000–1500 ºC in crucibles. Phase formation occurs by solid state reaction at high temperature. The solid state reaction which requires high synthesis temperature is time-consuming and is not environmentally friendly due to its high energy consumption. Therefore, the synthesis methods of these materials at much lower temperatures to decrease the energy cost and the reaction time are of interest.

1.4. Molten Salt Synthesis (MSS)

Liu et al. [6] gave a detailed review on molten salt synthesis. They concluded that the solid state reaction rate is limited by the slow diffusion of the solid reactants. However, reactions in a molten salt can occur at a much lower temperature with faster mass transfer transport due to its high viscosity and shorter diffusion distance. Besides, salts are easily dissolved in water and therefore it is easy to separate the product from salts for isolation. Salts are also advantageous because they are not volatile. When choosing a molten salt system, it is important to choose the one which does not react with the precursor materials. Alkaline metal chlorides (Lithium Chloride, Potassium Chloride and Sodium chloride) are a good choice for the precursors being used in this study. In this thesis, Lithium Chloride (LiCl) and Potassium Chloride (KCl) are being used because the LiCl-KCl salt system has a lower eutectic melting temperature than the NaCl-KCl salt system.

1.5. Scope of this thesis

Solid state reaction, combustion synthesis and sol-gel method have been explored in previous studies to prepare powders. This study aims to use molten salt synthesis method as an alternative way to form certain perovskite materials at lower temperature instead of high temperature solid state reaction. These particles are then used as reactants in a second molten salt synthesis step to form the core-shell structure. The molten salt method besides decreasing the synthesis temperature can also be used to control the composition of the particles and the structures formed.

In Chapter 2, we summarize the formation of $LaCrO_3$, $LaMnO_3$ and LSCF particles in eutectic molten salts in air at low temperatures. Expected $LaCrO_3$, $LaMnO_3$ and LSCF particles are successfully formed in a homogeneous growth as the promising SOFC interconnect or cathode materials.

In Chapter 3, the formation of core-shell structured particles using the core particles formed in Chapter 2 is described. With the molten salt method, the shell nucleates via heterogeneous nucleation in contrast to the synthesis of single phase particles which form through homogeneous nucleation. It is shown that core-shell particles are formed through heterogeneous route. In the final product, $LaCrO_3$ and LSCF core particles are surrounded by the $LaMnO_3$ shell. The particle size and structure of core-shell particles were also investigated.

Conclusions are presented in Chapter 4 and further suggestions for this work are presented in Chapter 5.

2. MOLTEN SALT SYNTHESIS OF LANTHANUM MANGANITE, LANTHANUM CHROMITE AND LSCF

2.1. Introduction

$LaMnO_3$ and $LaCrO_3$ based perovskite oxides can be used as the cathode and interconnect materials in SOFCs (Solid Oxide Fuel Cells), respectively. They have high electrical conductivity and good chemical stability in both fuel and oxidant environments. Conventionally, they are prepared at very high temperature, i.e. 1200 ºC, using solid state reaction [7,8], combustion method [2,9,10], sol-gel method [12] or hydrothermal synthesis [13,14]. Gupta and Tiwari et al. [7,8] synthesized $LaCrO_3$ using solid state reaction at 1300–1650 ºC for 24h. It is time-consuming and it costs a lot of energy during the heating process. Also it was shown that $LaCrO_3$ cannot sinter very well at high temperature due to the high vapor pressure of chromium. Hernandez [2], Khetre [9] and Park et al. [10] used the combustion method to synthesize $LaMnO_3$ and $LaCrO_3$. Manganese (II) nitrate tetrahydrates, $Mn(NO_3)_2.4H_2O$, Chromium nitrate nonahydrates, $Cr(NO_3)_3.9H_2O$ and Lanthanum nitrate hexahydrates, $La(NO_3)_3.6H_2O$ were used as precursors. These precursors and a required organic fuel, for example glycine, are mixed and combusted to form a fine product with high surface area of the target phase. The combustion is rapid, spontaneous and self-sustaining [11]. However, the nitrate precursors are expensive and the final product is often not fully phase pure with some residues due to the short reaction time. Besides, it still requires a final high temperature step to complete phase formation and obtain densified powders [10]. Zhigalkina et al. [12] used the sol-gel method to synthesis $LaCrO_3$. However, they encountered solubility challenges of the Lanthanum

nitrate, $La(NO_3)_3$ and Chromium nitrate, $Cr(NO_3)_3$ reagents in the PVA polymer solvent as a gel. Hydrothermal synthesis was used by Zheng and Kang et al. [13,14] to synthesize $LaCrO_3$ powder with a particle size range from 100nm to 3μm. During the preparation, the precursor slurry needed to be heated at 260 ºC for 7 days and required long-time stirring, which is time-consuming. The results were also affected by the KOH alkalinity as a precipitant. Ding et al. [15] used the EDTA-citrate polymerized complexing process to form doped $LaCrO_3$ perovskite. This process has to strictly control pH values after adding citric acid.

LSCF is attracting more and more interest as an ideal cathode material for SOFC due to its excellent electrical and thermal performance. It can be prepared by various synthesis methods. Conceicao et al. [16] prepared LSCF by the combustion synthesis route and evaluated the microstructure of LSCF powders. Using this method, nanoscale particles of LSCF (size range: 9–20nm) can be synthesized but it generates organic residues and secondary phases powders (La_2O_3, $SrCO_3$ and $FeCO_3$) after combustion due to the incomplete process in a short reaction time. Further, the powders easily agglomerate.

2.1.1. Kinetics of Molten Salt Synthesis

The purpose of the molten salt method is to eliminate the disadvantages mentioned above. Molten salt method can accelerate the kinetics of the formation by orders of magnitude to faster reach the equilibrium state. It enhances the interdiffusion between two reacting species for the liquid state, which is millions of times faster than in the solid state.

For the mechanism of the solid-state reaction, La^{3+} ions from the La_2O_3 need to

transport to the interface of the oxide particles and then diffuse into the Cr_2O_3 or Mn_2O_3 solid solution. Cr^{3+} or Mn^{3+} ions would also transport and diffuse into the La_2O_3 solid solution. All of this diffusion occurs through solid state diffusion which is kinetically slow. Then it forms a $LaCrO_3$ or $LaMnO_3$ reaction layer. This can be evidenced by the position of a Pt marker in the vicinity of the interface [17].

However, when molten salt is used as the solvent in the molten salt synthesis. The reactants will dissolve into the molten salt liquid and become La^{3+}, Cr^{3+} or Mn^{3+} ions. The molten salt would increase the contact area and mass transport to let the ions have a better contact and combine. The contact positions and spots in the solid state reaction are more limited. Besides, the mobility of species in the molten salt can be reached to 10^{-5} – 10^{-8} cm^2sec^{-1}, which is much larger than that in the solid state reaction (10^{-18} cm^2sec^{-1}). This provides a quicker formation rate of the final product [18–20].

According to Kimura's research [21], molten salt synthesis narrows the fluctuation and distribution of the composition, which indicates synthesized particles are more homogenous than those formed by solid state reaction. Moreover, agglomeration happens a lot in the solid state reaction. In contrast, molten salt synthesis can prevent and eliminate the neck growth of product to lower the agglomeration. Thus, it's easy to control the particle size and shape by using the molten salt synthesis.

2.1.2. Thermodynamics of Molten Salt Synthesis

The formation of the product particles contains two steps: the chemical reaction and the growth of particles [22–24]. The solid state reactants will firstly dissolve and become

solvated as La^{3+}, Cr^{3+} or Mn^{3+}, O^{2-} ions in the molten salt liquid phase, as shown in equation (1-4).

$$La_2O_3\,(s) \rightleftharpoons La_2O_3\,(l) \quad (1)$$

$$Mn_2O_3\,(s) \rightleftharpoons Mn_2O_3\,(l) \quad (2)$$

$$La_2O_3\,(l) \rightleftharpoons La^{3+} + O^{2-} \quad (3)$$

$$Mn_2O_3\,(l) \rightleftharpoons Mn^{3+} + O^{2-} \quad (4)$$

Then these ions would contact and combine with each other [25].

$$La^{3+} + O^{2-} \rightleftharpoons (LaO)^{+} \quad (5)$$

$$M^{2+} + O^{2-} \rightleftharpoons (MO_2)^{-} \quad (6)$$

Then Lanthanyl cation would react with Manganese cation to form perovskite oxides according to Equation (7) [25].

$$(LaO)^{+} + (MO_2)^{-} \rightleftharpoons LaMnO_3\,(l) \quad (7)$$

The overall reaction can be expressed as:

$$La_2O_3\,(l) + Mn_2O_3\,(l) \rightarrow LaMnO_3\,(l) \quad (8)$$

Then $LaMnO_3$ in liquid solution is precipitated as solid once its solubility is exceeded.

$$LaMnO_3\,(l) \rightleftharpoons LaMnO_3\,(s) \quad (9)$$

The chemical potential in the solid state is given by:

$$\mu_{LaMnO3(s)} = \mu^0_{LaMnO3(s)} + RT \ln a_{LaMnO3(s)} \quad (10)$$

$$\text{or} \quad \mu_{LaMnO3(s)} = \mu^0_{LaMnO3(s)} \text{ due to } a_{LaMnO3(s)} = 1 \quad (11)$$

And that in the liquid solution is given by,

$$\mu_{LaMnO3(l)} = \mu^0_{LaMnO3(l)} + RT \ln a_{LaMnO3(l)} \quad (12)$$

At equilibrium:

$$\mu_{LaMnO3(s)} = \mu_{LaMnO3(l)} \quad (13)$$

Substituting Equation (11) and (12) into (13),

$$\mu^0_{LaMnO3(s)} = \mu^0_{LaMnO3(l)} + RT \ln a_{LaMnO3(l)} \quad (14)$$

The thermodynamic activity can be expressed as below:

$$a_i = \gamma_i * x_i \quad (15)$$

Where γ is the activity coefficient of species i and x is the mole fraction, which means the solubility of species i in this case. Combining Equation (14) and (15), the only influence factor limiting the reaction is the unavoidable solubility of the precursors oxides in the molten salt liquid.

Although the solubility for $LaMnO_3$, $LaCrO_3$ and LSCF cannot be found directly, the solubility of several oxides in the molten alkali fluorides or chlorides has been previously studied [26–31]. Table.2 gives the solubility of different oxides in the molten NaCl-KCl eutectic at around 700 ºC, which can be used as a reference [29,30].

Oxides	Solubility (mol%)
La_2O_3	1.5
Mn_2O_3	0.055
Cr_2O_3	0.08
Fe_2O_3	0.0065
Co_3O_4	0.075
SiO_2	0.5
NiO	0.06
MgO	0.06
CaO	0.035
Al_2O_3	0.07

Table 2. The solubility of different oxides

The solubility data indicate that the solubility of the oxides is extremely small and will not greatly change the overall target stoichiometry of the product. Further, the solubility decreases with a decreasing molten salt temperature. This indicates that although very small amount of solids may dissolve in the liquid, most reactants will not react with salts and directly precipitate the desired solid product at such low temperatures.

2.1.3. La_2O_3-Mn_2O_3-Molten Salt Pseudo Phase Equilibria

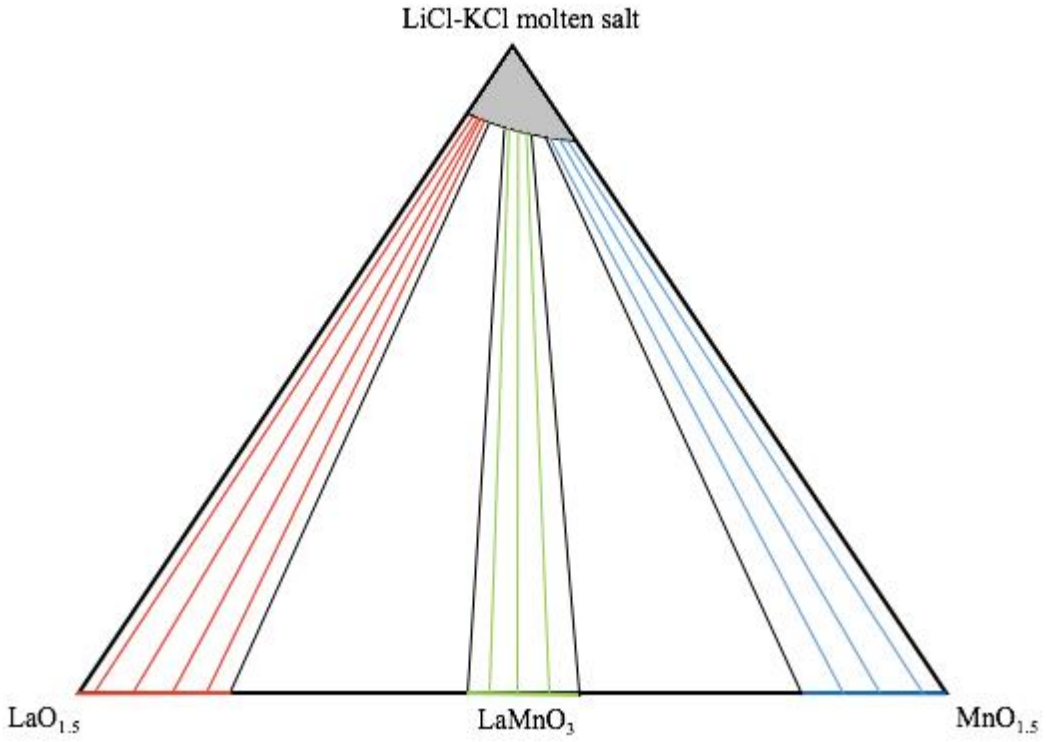

Fig. 3. Pseudo ternary phase equilibria in La_2O_3 - Mn_2O_3 –molten salts system at 500°C in air

A schematic of the potential Pseudo Ternary phase equilibria in La_2O_3- Mn_2O_3-molten salt system at 500 ºC in air is shown in Fig. 3. The equilibrium phase of $LaMnO_3$ is a solid state solution of La_2O_3 and Mn_2O_3 mixture with a small range of compositions. The grey area is the single liquid phase of molten salt with dissolved $LaO_{1.5}$ and $MnO_{1.5}$. The red pseudo-binary tie lines show the two phase region of the La_2O_3 solid solution and molten salt liquid phase. The blue pseudo-binary tie lines show the two phase region of Mn_2O_3 solid solution and molten salt liquid phase. The green pseudo-binary tie lines show the two phase region containing $LaMnO_3$ (with variable stoichiometry) solid solution and the molten salt liquid phase. The target perovskite composition and its equilibrium with the

liquid phase is expected to be in this green region based on the starting precursor ratios chosen. The white areas are the triple phase regions of one liquid phase and any two solids solutions.

Moreover, the Gibbs's phase rule can be used to understand the phase equilibria in the La_2O_3- Mn_2O_3- $LaMnO_3$ system.

$$F= C-P+2 \quad (16)$$

In this equation, F represents the number of degree of freedom, C is the number of components and P is the number of phases in the equilibrium state. The number of components is three in this case, namely, the salt (here simplified as one component), La_2O_3 and Mn_2O_3. Since temperature and the overall pressure are both fixed, the total number of remaining degrees of freedom is just 3-P. Thus, a maximum of three phases can be in equilibrium. In the proposed schematic phase diagram, regions of single phase, two phase, and three phase equilibria are all to be found.

$$F= 3-P+2 \text{ or } F= 5-P \quad (17)$$

However, further work may be required to determine the exact composition of La_2O_3 and Mn_2O_3 needed to successfully form the target $LaMnO_3$ composition.

2.1.4. The feasibility of molten salt synthesis

The molten salt synthesis is much simpler with less reaction time and residual impurities. The agglomeration of particles can also be prevented by the molten salt medium. Romero et al. [32] synthesized $AFeO_3$ system (A=La,Gd). Gopalan et al. [33] synthesized perovskite oxides solid solutions of $BaTiO_3$-$SrTiO_3$ and $BaZrO_3$-$SrZrO_3$. Li

and Huang et al. [34–36] synthesized $LaAlO_3$, $La_2Zr_2O_7$ and $La_{9.33}Si_6O_{26}$ powders, respectively. They all used the molten salt method at intermediate temperatures, which proves the feasibility of molten salt synthesis to form complex higher order oxides. $LaMnO_3$ was successfully synthesized in the molten chlorides by Vradman et al. [37] in previous work. He reported $LaMnO_3$ formed in molten NaCl-KCl and LiCl-KCl eutectic mixtures by using the nitrates as precursors at 600 ºC. The same $LaMnO_3$ has also been synthesized in molten alkali metal nitrates ($NaNO_3$ –KNO_3) by Matei et al [25].

In this study, $LaMnO_3$, $LaCrO_3$ and LSCF particles were also synthesized by the molten salt method at a much lower temperature using inexpensive precursors and molten chlorides salt system. Structure and particle size characterization was performed using X-ray Diffraction (XRD) and Scanning Electron Microscopy (SEM).

2.2. Experiments

2.2.1. Molten salt synthesis of Lanthanum Manganite

2.2.1.1. Synthesis of $LaMnO_3$

Lanthanum oxide, La_2O_3 and Manganese (III) oxide, Mn_2O_3 (Alfa Aesar, purity= 99.9% and 98%) were used as the reactants. In order to reduce the particle size and achieve homogenization, mixtures of precursor powders La_2O_3 and Mn_2O_3 in an appropriate stoichiometric ratio were ball milled in ethanol for 2h using zirconia milling media (SPEX SamplePrep 8000 M Mixer/Mills). Zirconia balls were removed by sieving. Then the well mixed and milled precursors suspensions were dried in an oven at 80 ºC overnight. A mixture of LiCl and KCl (Alfa Aesar, purity= 99%) was chosen as the molten salts, which

has a lower melting temperature than NaCl-KCl salts system (50%: 50%, 658 ºC) [38]. The eutectic point of LiCl-KCl (59.2%: 40.8%) system is 353 ºC [39]. Such low temperature can prevent the formation of $LaMnO_3$ to begin by the solid state reaction.

Precursor powders and salts were placed in the crucibles and heated in a box furnace at 370 ºC, 400 ºC, 450 ºC, 500 ºC and 550 ºC for 8h in air with 5 ºC/min heating rate. After cooling down to room temperature, LiCl-KCl molten salt was dissolved and washed away with distilled water several times. The synthesized $LaMnO_3$ powders were dried in an oven at 80 ºC overnight.

2.2.1.2. Characterization

The X-ray diffraction patterns of $LaMnO_3$ powders were obtained by Bruker D8 instrument using Cu-Kα radiation. The scan range of 2θ was set between 20° to 90° in the continuous scan mode. The scanning step width of 2θ was 0.01° and the scan rate was 0.3 seconds for each step. The Scanning Electron Microscopy (SEM) images and Energy Dispersive X-ray spectroscopy (EDS) element analysis and mapping were performed using Zeiss Supra55VP Field Emission SEM (FESEM) instrument.

2.2.2. Molten salt synthesis of Lanthanum Chromite

2.2.2.1. Synthesis of $LaCrO_3$

Lanthanum oxide, La_2O_3 and Chromium oxide, Cr_2O_3 (Alfa Aesar, purity= 99.9% and 99%) were used as precursors materials. They were SPEX ball mixed using zirconia milling ball in ethanol for 2h. After drying in an oven at 80 ºC for overnight, the mixed precursor powders were then mixed with a eutectic composition of LiCl-KCl (mixing ratio

= 59.2mol%: 40.8mol%) salt and placed in a crucible. The crucible was placed in a box furnace and heated to various temperatures (370 ºC, 400 ºC, 450 ºC, 500 ºC, 550 ºC and 600 ºC) for 8h in air with 5 ºC/min heating rate. Then the synthesized $LaCrO_3$ powders were washed with distilled water at room temperature to wash away the LiCl-KCl salts and dried in the oven overnight.

2.2.2.2. Characterization

The characterization methods for the $LaCrO_3$ product were identical to the $LaMnO_3$.

2.2.3. Molten salt synthesis of 40% strontium doped lanthanum cobalt iron oxide(LSCF)

2.2.3.1. Synthesis of $La_{0.6}Sr_{0.4}Co_{0.2}Fe_{0.8}O_3$ (LSCF-6428)

The formation of LSCF happened in the eutectic composition of LiCl-KCl (mixing ratio = 59.2mol%: 40.8mol%) molten salt system as well. The precursors were Lanthanum oxide (La_2O_3), Cobalt (II, III) oxide (Co_3O_4), Iron (III) oxide (Fe_2O_3) and Strontium carbonate ($SrCO_3$). They were all purchased from Alfa Aesar with purity over 99%. The method of synthesis was identical to the $LaMnO_3$ and $LaCrO_3$ powders.

2.2.3.2. Characterization

The XRD patterns of LSCF were measured by Bruker D8 instrument using Cu-Kα radiation. The microstructure and particle size of LSCF powders was investigated by Zeiss Supra55VP Field Emission SEM (FESEM) instrument.

2.3. Results and Discussions

2.3.1. Results of Lanthanum Manganite($LaMnO_3$)

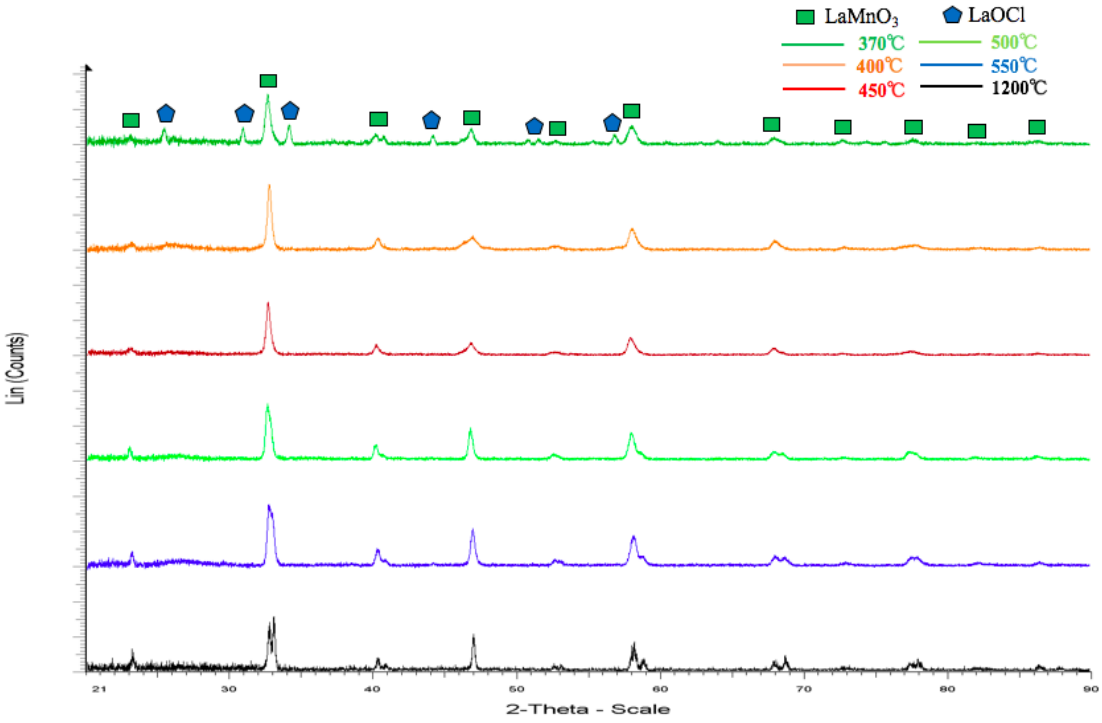

Fig. 4. X-ray diffraction patterns of $LaMnO_3$ at different synthesis temperatures (370ºC, 400ºC, 450ºC, 500ºC and 550ºC for 8h in air) Note: the inclusion of the XRD pattern obtained after solid state synthesis at 1200°C for 8h.

X-ray diffraction patterns of $LaMnO_3$ synthesized by the molten salt method at different synthesis temperature for 8h are presented in Fig.4. A solid state reaction at 1200 ºC for 8h was also performed as a comparison. The XRD pattern for reaction at 370 ºC shows 2nd phase indexed to Lanthanum Oxychloride (LaOCl) besides the $LaMnO_3$ phase. LaOCl is expected as the product of the reaction between molten chloride salts and dissolved La_2O_3 in the liquid. While all other results show the complete formation of the new phase, pure $LaMnO_3$ with no more La_2O_3 or Mn_2O_3 peaks to be seen at 400 ºC or above. The XRD patterns are consistent with the powder formed by the solid state reaction.

It should be noted that there is a trend of peaks splitting as the reaction temperature increases. All of the peaks for reactions at 400 ºC and 450 ºC are single peaks, while reactions at 500 ºC and 550 ºC start to show double peaks at certain 2θ values, for example when 2θ=32.37° for the (011) peak, 2θ=57.74° for the (112) peak and 2θ=67.77° for the (022) peak. The solid state reaction at 1200 ºC shows the greatest amount of splitting. Single peaks corresponded to cubic perovskite structures. The splitting of XRD peaks can be ascribed to the existence of hexagonal structures which are stable at higher temperatures. The formation of hexagonal particles with the increasing reaction temperature is thus consistent with the known crystal structure of $LaMnO_3$. The $LaMnO_3$ powder is therefore a mixture of particles with cubic and hexagonal structures. However, no hexagonal particles are observed in the SEM images of $LaMnO_3$ synthesized by the molten salt method. For example, the SEM image of the particles formed at 500 ºC, as shown in Fig. 5, only shows cubic shaped particles of $LaMnO_3$ with an average size around 500 nm. Maybe the hexagonal particles are too small to be seen. Thus, a longer reaction time may be needed for further observation of the hexagonal structure.

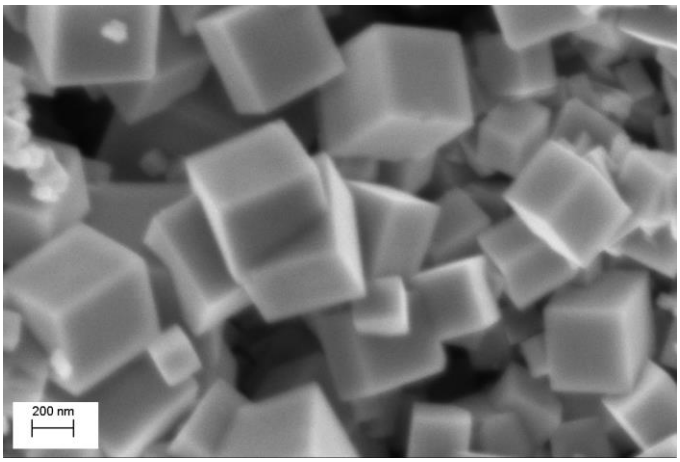

Fig. 5. SEM image of $LaMnO_3$ particles synthesized at 500ºC

To prove the necessity of the molten salt to synthesize $LaMnO_3$ at the low synthesis temperature of 500ºC, a reaction of La_2O_3 and Mn_2O_3 was carried out without the LiCl-KCl salt system at 500 ºC for 8h. The XRD result (Fig.6 (a)) shows that no $LaMnO_3$ is formed. The peaks of the unreacted La_2O_3 and Mn_2O_3 reactants remain unchanged and some secondary phases ($LaMn_2O_5$ and La_2MnO_5) appeared, which was expected as the intermediate phase in the incomplete solid state reaction. $LaMnO_3$ prepared by the molten salt method at 500 ºC and by solid state reaction at 1200 ºC is also shown in Fig.6 (b) (c) as a comparison. Therefore, LiCl-KCl molten salt system played a key role in enabling and accelerating the formation of $LaMnO_3$ at 500ºC.

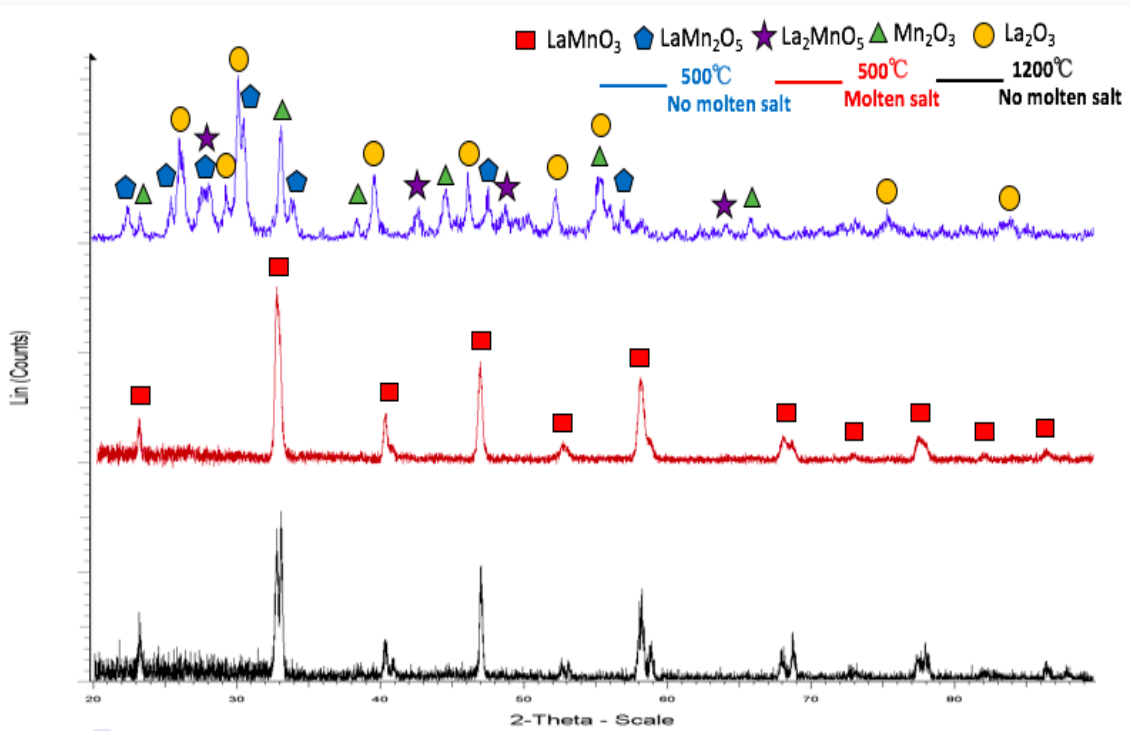

Fig. 6. X-ray diffraction patterns of mixed powder at various reaction situations for 8h: (a) 500ºC without molten salt; (b) 500ºC with molten salt; and (c)1200ºC without molten salt

2.3.2. Results of Lanthanum Chromite($LaCrO_3$)

The formation of $LaCrO_3$ synthesized by the molten salt method at different synthesis temperatures (370–600^oC) for 8h in air was also studied and compared with LaCrO3 formed by solid state reaction. The results are characterized by X-ray diffraction shown in Fig. 7. $LaCrO_3$ was successfully formed at all temperatures. A second phase of LaOCl was found in addition to the $LaCrO_3$ perovskite at all reaction temperatures during the formation process. This result shows the intrinsic interaction of the salt with the products. Although the salts reacted with the precursors, expected $LaCrO_3$ can still be synthesized. Besides, LaOCl peak intensity decreases as the temperature increases, which means LaOCl phase becomes less stable at higher temperatures and single phase $LaCrO_3$ becomes more stable. LaOCl may convert back into insoluble La_2O_3 by a reaction with oxygen at higher temperature [40]. The reaction equation is shown below.

$$LaOCl + O_2 \rightarrow La_2O_3 + Cl_2 \quad (18)$$

The oxides would then continuously react to form more product.

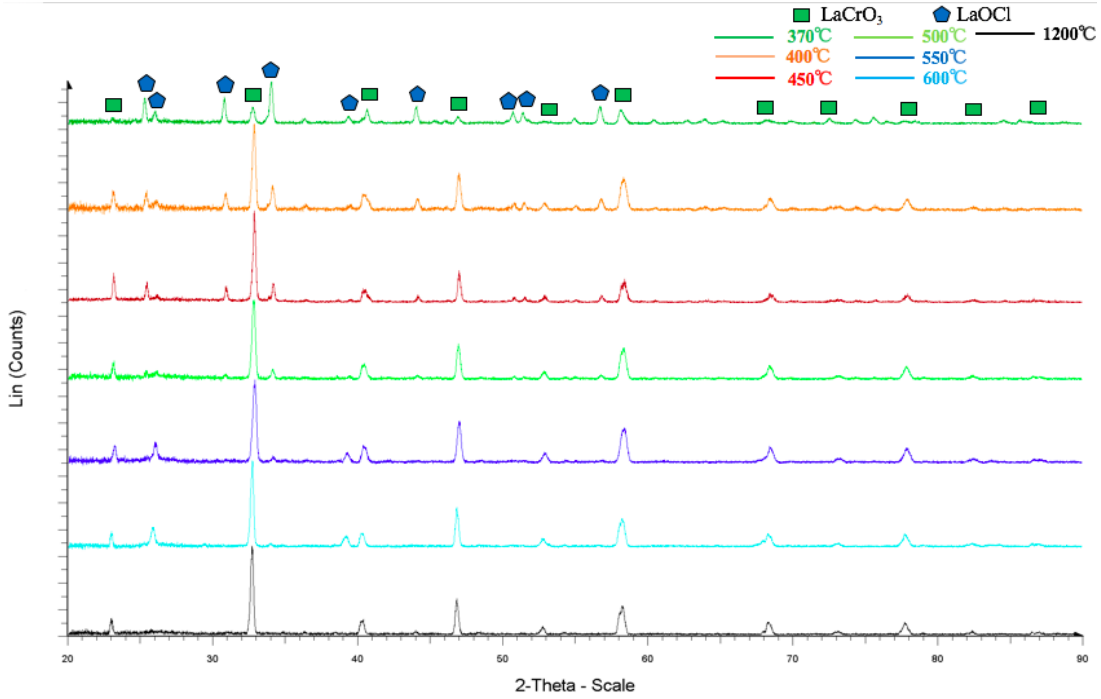

Fig. 7. XRD patterns for $LaCrO_3$ at 370ºC, 400ºC, 450ºC, 500ºC, 550ºC, 600ºC and 1200ºC for 8h. Also shown is the pattern for $LaCrO_3$ formed using the solid state reaction method at 1200ºC for 8h.

XRD patterns of $LaCrO_3$ at different synthesis temperatures in air are similar to the $LaMnO_3$ patterns in the previous section (2.3.1). The peaks have a splitting trend at higher temperatures, for example as shown in Fig. 7 when the peak corresponding to 2θ=58.23° for the (211) peak. This indicates the hexagonal crystal structure stabilizes at higher temperatures. To get a better understanding of the change in crystal structure from 370 ºC to 600 ºC, the XRD patterns was magnified as shown in Fig. 8 for 2θ= 57–59° to show the (321) peak splitting, which corresponds to 2θ=58.23°. It shows only cubic structures were formed at low temperature (for example, 400 ºC) and then hexagonal phase starts to appear at 450 ºC. Also, the split of peaks becomes more obvious with an increase in synthesis temperature. Therefore, $LaCrO_3$ has the structural transition from cubic to hexagonal structures at higher temperatures.

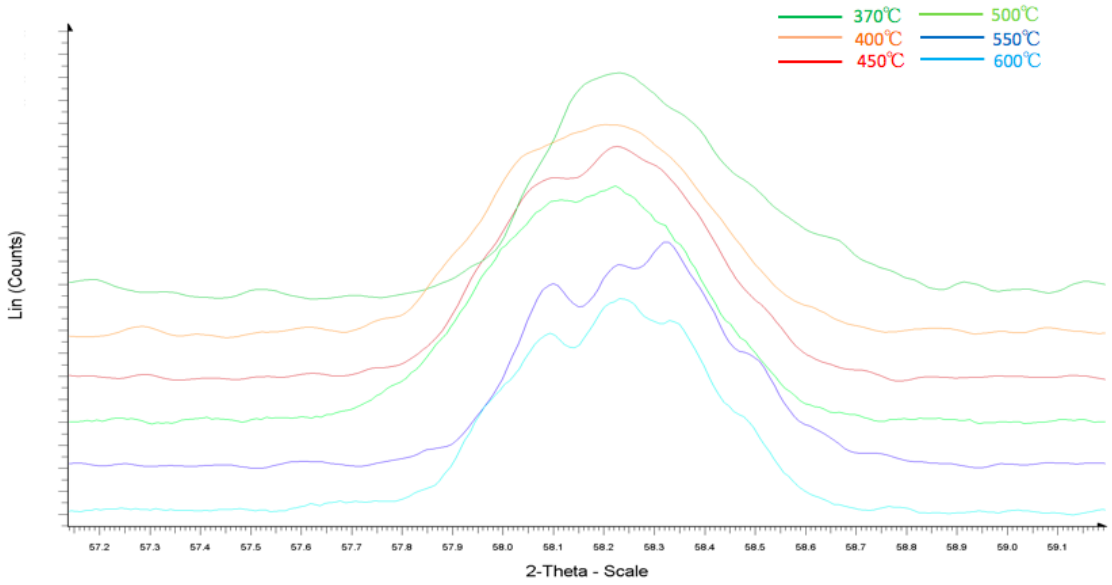

Fig. 8. Magnified XRD patterns for $LaCrO_3$ between 370ºC and 600ºC, for 2θ= 57–59°

This structure transformation has been further confirmed by the SEM images (Fig.9 (a) (b)), for example, the reaction at 400 ºC and 500 ºC. Only cubic shaped crystals are found when synthesized at 400 ºC, but some hexagonal particles are observed at 500 ºC.

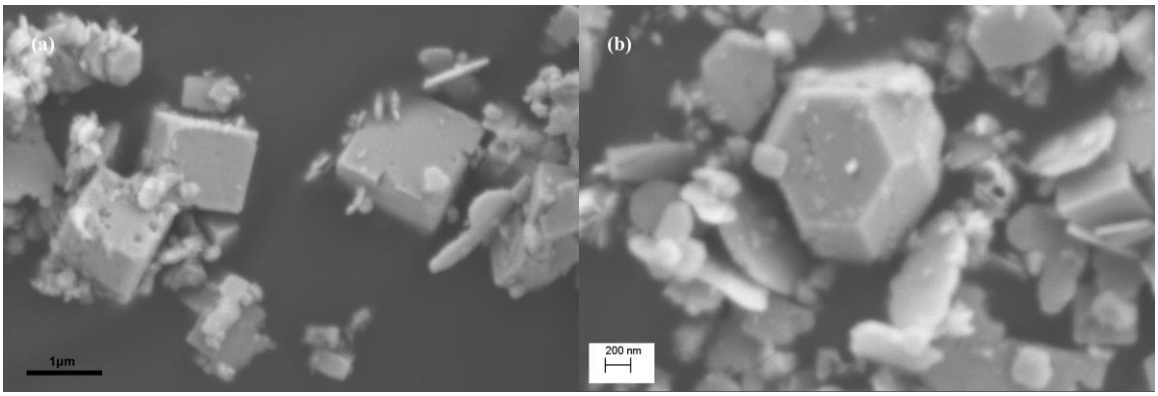

Fig. 9. SEM images of $LaCrO_3$ synthesized at (a) 400 ºC (b) 500 ºC

Fig. 10 (a) (b) shows the coexistence of cubic and hexagonal phase at the same synthesis temperature (550 ºC). The shape and size of particles were distributed randomly. This result can be explained as being due to incomplete transformation from the cubic to the hexagonal phase. Longer reaction time may be needed for further study.

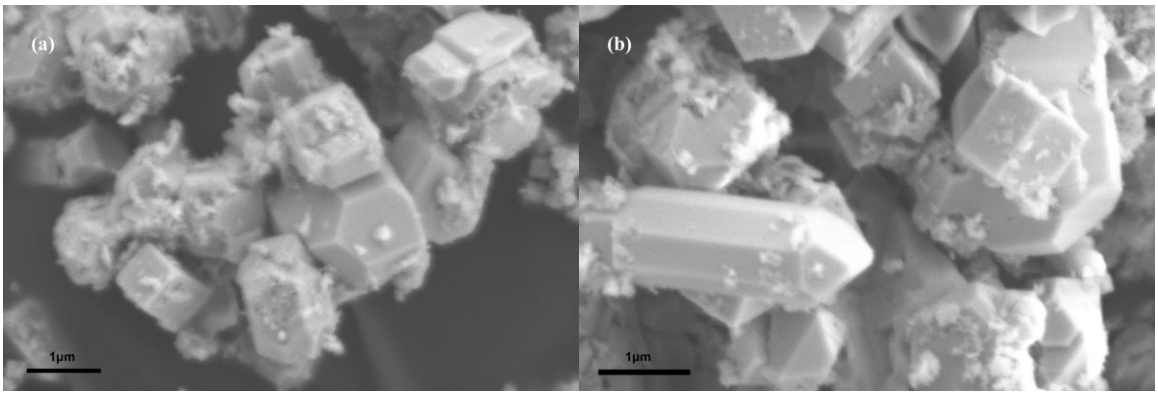

Fig. 10 (a) (b). SEM images of $LaCrO_3$ synthesized at 550ºC

To understand the role of the salt system in the molten salt synthesis method, reactions of La_2O_3 and Cr_2O_3 were carried out with or without the LiCl-KCl salt system at 500 ºC for 8h. In Fig.11, $LaCrO_3$ is successfully formed through the molten salt synthesis method at 500 ºC and through solid state reaction at 1200 ºC. However, when the reaction happens at 500 ºC without salt, La_2O_3 and Cr_2O_3 peaks can still be seen. That means La_2O_3 and Cr_2O_3 powders without the molten salt system will not have the reaction to form $LaCrO_3$ at low temperature (500 ºC). There are some La_2CrO_6 peaks shown on the XRD patterns, which is considered as an intermediate phase in the incomplete formation of $LaCrO_3$ through solid state reaction. This result once again shows the importance of LiCl-KCl molten salt system in enabling and accelerating the formation of $LaMnO_3$ at a relatively low temperature.

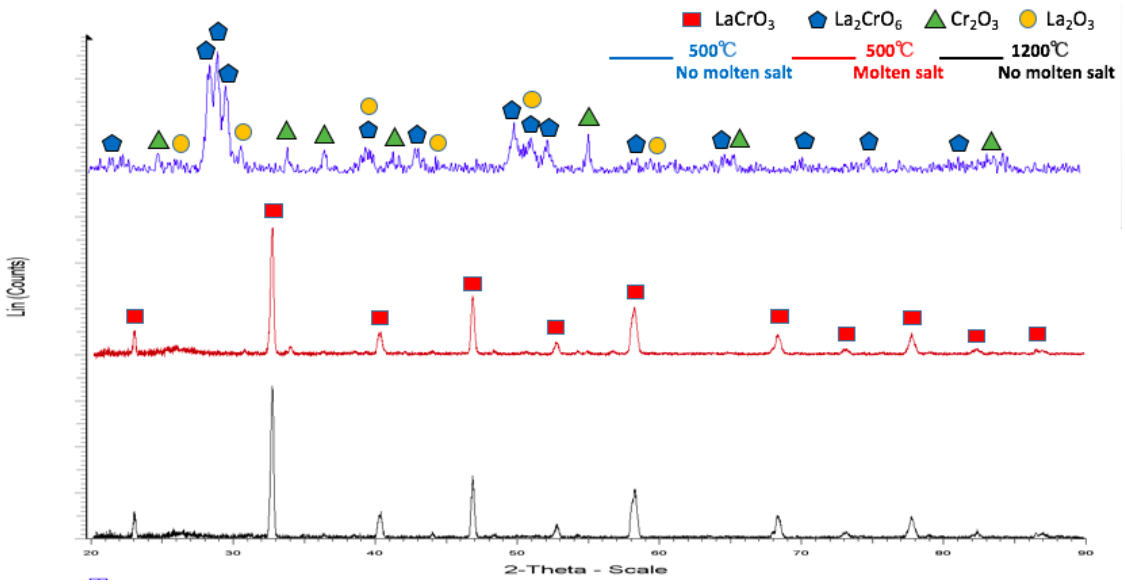

Fig. 11. X-ray diffraction patterns of mixed powders (La_2O_3 and Cr_2O_3) reacted results at various reaction situations for 8h: (a) 500°C without molten salt; (b)500°C with molten salt; and (c)1200°C without molten salt

2.3.3. Results of $La_{0.6}Sr_{0.4}Co_{0.2}Fe_{0.8}O_3$(LSCF-6428)

From the X-ray diffraction results shown in Fig. 12, it is suggested that LSCF particles can be homogenously synthesized by the molten salt method at temperatures as low as 500 ºC with overall cubic structures, as confirmed in the SEM image shown in Fig. 13. The average size of crystallites was 600 nm. No further experiments at different reaction temperatures were done since it has already proved the successful formation of LSCF at 500 ºC.

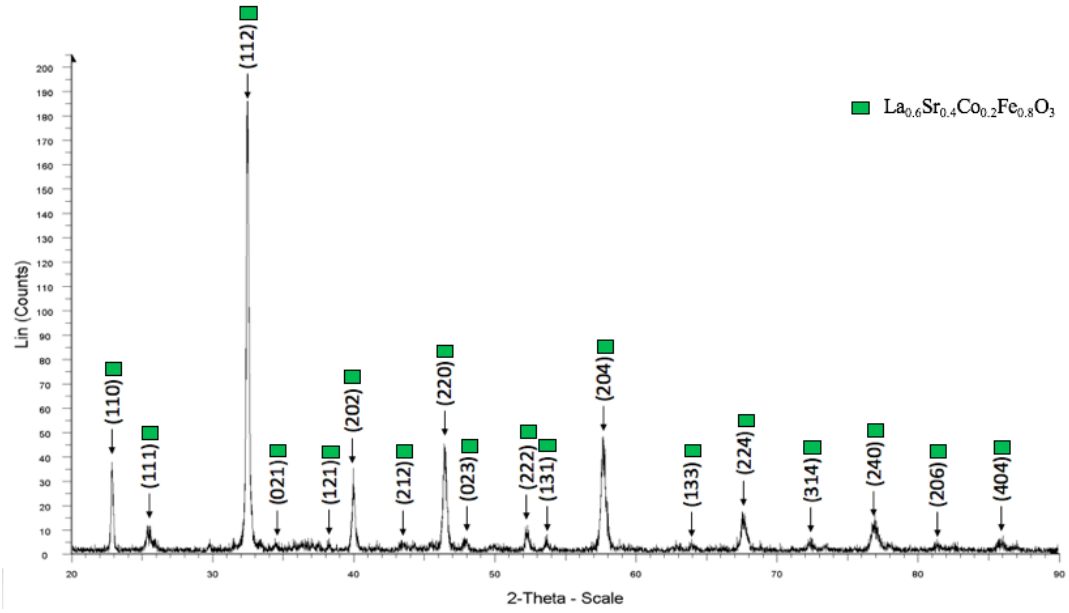

Fig. 12. X-ray diffraction pattern of LSCF synthesized at 500°C

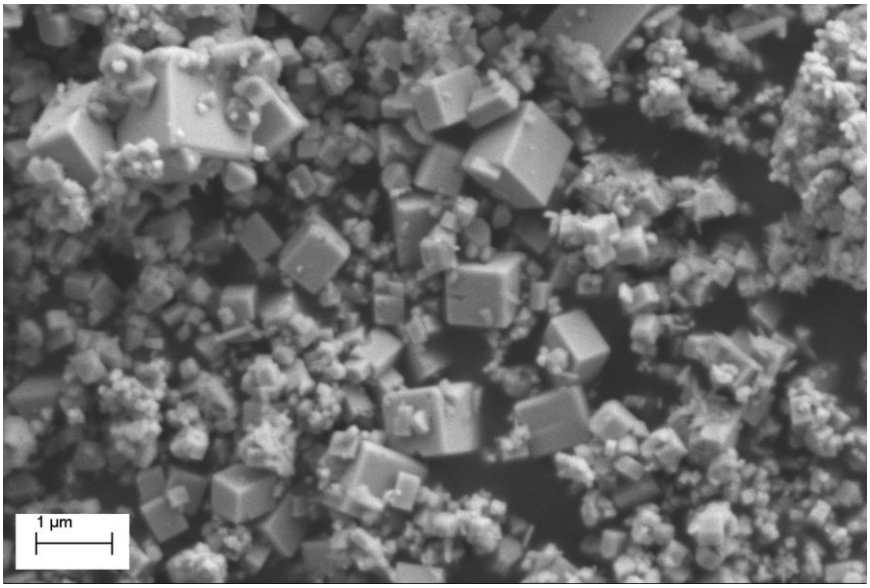

Fig. 13. SEM image of LSCF synthesized at 500°C

Similar experiments were performed without the presence of the molten salt and they clearly indicate the non-formation of the LSCF phase at 500°C. It provides conclusive evidence on the role of the molten salt to accelerate perovskite phase formation kinetics, as shown in Fig. 14.

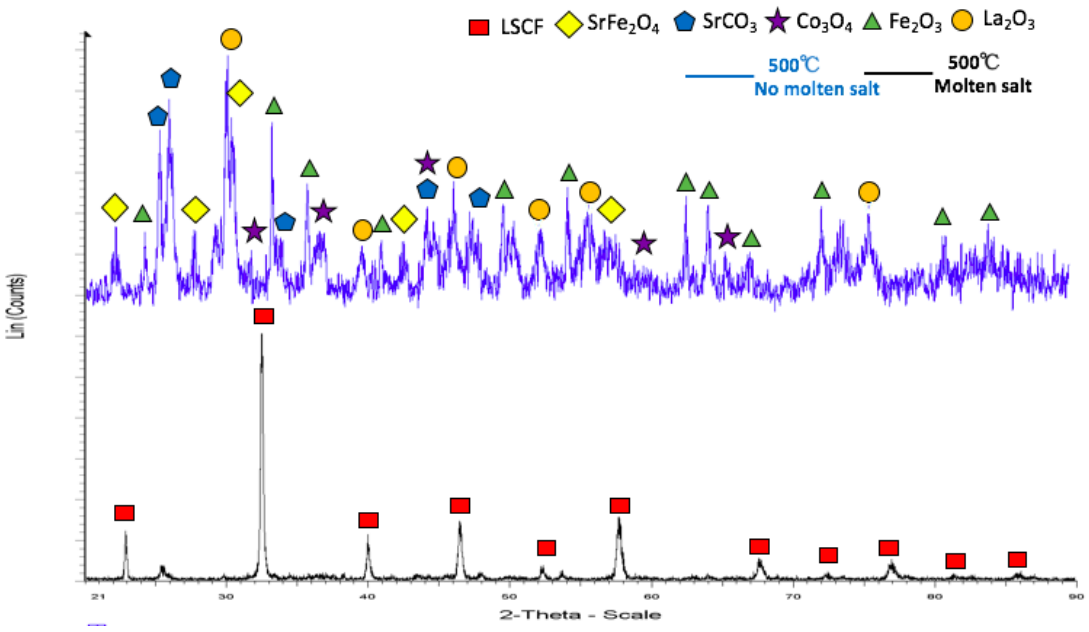

Fig. 14. X-ray diffraction patterns of mixed powders (La_2O_3, Fe_2O_3, $SrCO_3$ and Co_3O_4) reacted results at various reaction situations for 8h: (a) 500°C without molten salt; (b)500°C with molten salt

2.4. Conclusions

X-ray diffraction patterns and SEM images show that $LaMnO_3$ and $LaCrO_3$ perovskite can be completely formed at low temperature (400 °C), but when forming $LaCrO_3$, there is a by-product of LaOCl. However, LaOCl peaks disappear at higher temperatures. LSCF can be successfully synthesized at 500 °C in the molten salt. SEM microstructures show the $LaMnO_3$ and LSCF particles have a cubic symmetry, which was also verified by X-ray diffraction. Cubic $LaCrO_3$ transforms into a hexagonal structure above 450 °C. Then $LaCrO_3$ has the coexistence of both cubic and hexagonal phases which has also been verified by XRD. In summary, the molten salt method is an attractive low temperature alternative route for the synthesis of perovskite materials of interest as SOFC cathodes and interconnects.

3. MOLTEN SALT SYNTHESIS OF $LaCrO_3$-$LaMnO_3$ AND LSCF-$LaMnO_3$ CORE-SHELL PARTICLES

3.1. Introduction

The synthesis of core-shell particles has two main steps which can be achieved by a variety of methods. First of all, the core particles need to be formed with a certain size range. Impurities in core particle should be avoided. Then the particle shells can either grow on the surface of those core particles or be coated on to improve the phase contiguity and to isolate the core. The uniformity and thickness of shell needs to be controlled.

In the previous study, Lee et al. [41] synthesized $La_{0.6}Sr_{0.4}Co_{0.2}Fe_{0.8}O_3$ (LSCF)-$Sm_{0.2}Ce_{0.8}O_{2-d}$ (SDC) core-shell type powder at an intermediate temperature around 500 ºC –700 ºC. They used a polymerizable complex method which occurred in a polymeric resin to mix and calcinate the composite particles. The created core-shell particles had increased long-term stability with lower interfacial polarization resistance (0.265 Ωcm^2 at 650 ºC) compared with bare particles. However, this method involves the use of polymer resin, which is expensive and is not environmentally friendly. Liu et al. [42] synthesized Fe_2O_3-SnO_2 core-shell nanoparticles using a mixed lithium molten salt system (LiCl and $LiNO_3$). The electrochemical performance of the core-shell structures was enhanced compared to pure Fe_2O_3 particles which are used as the anode materials. This is because the transport length of ions and electrons gets shorter and electrical conductivity gets better when the Fe_2O_3 core is surrounded by the conductive shell (SnO_2). The results also showed that the core-shell particles have a higher discharge capacity of 664.8 mAh/g and smaller ohmic resistance of 75 Ω which is much better than the pure Fe_2O_3 particle (97.5 mAh/g and 150

Ω) and pure SnO_2 particle (59.5 mAh/g). Core-shell $BaTiO_3$ was fabricated through the molten hydrated salt method by Tian et al. [43]. The completed reaction was achieved in a short time with dispersive powders in comparison to a conventional hydrothermal method. This may because molten hydrated salts are viscous, which provides a shorter diffusion distance and prevents agglomeration. Alaparthi et al. [44] synthesized $(La_{1-x}Eu_x)_2Zr_2O_7$-YBO_3 spherical core-shell nanoparticles using sol-gel process. $(La_{1-x}Eu_x)_2Zr_2O_7$ core particles were first created by molten salt synthesis and then shell was added by sol-gel method. These particles were created for use as lighting devices and radiation detectors due to their excellent photocatalytic activity. However, in this research, the core-shell precursor particles still needed to be annealed at high temperature after the sol-gel process. This step caused the formation and agglomeration of some large-sized spherical particles. Core-shell $SrTiO_3/TiO_2$ heterostructure particles and La-/Rh- codoped $SrTiO_3$ core-shell particles were reported by Zhao and Wang et al. [45,46] using sacrificial template synthesis. Shell seems to have an epitaxial relationship with core due to the extraction of chemical bonds from core [47,48], which provides a better contact between core and shell. This core-shell structure improves the phase contiguity and reduces the band gap with gradient diffuse concentration and energy levels. Further, there are more electron-hole pairs due to decreasing the transport distance between holes and electrons. However, this method involves the synthesis of both template and core-shell particles and has too many steps. It is time-consuming and introduces byproducts in the solution during several hydrothermal treatments, which is energetically expensive. Nonetheless, all of these studies prove that a higher electrical conductivity and performance for core-shell particles can be obtained

compared with bare particles. In addition to application in electrical devices, core-shell $SrTiO_3$ particles can also be used in some biological applications due to their better biocompatibility and capacity rather than pure species [49]. For application in optical devices, core-shell Y_2O_3 nanoparticles and their luminescence properties were synthesized and studied [50]. The results showed a longer luminescent lifetime and a higher efficiency for its core-shell structure. Core-shell particles are also excellent catalysts to accelerate the chemical process with good thermal and chemical stabilities [51]. The shell on the surface isolates the catalytic core from the actual reaction, which prevents the core directly contacting with the reactants and products. This maintains the high catalytic activity of the core.

Considering the processing disadvantages above and trying to apply core-shell particles into the field of SOFC, this chapter investigates the preparation of core-shell particles using the molten salt method involving the heterogeneous nucleation and growth. I predicted heterogeneous nucleation of $LaMnO_3$ on the surface of a $LaCrO_3$ or LSCF core where the surfaces of core particles would become the nucleation sites for the growth of the shell.

To clarify homogeneous nucleation spontaneously, it happens at random sites in the bulk of the system and this causes a lack product uniformity [52–55]. Homogenous nucleation spontaneously happens at random sites and has difficulty for a uniform interior substance. Heterogeneous nucleation occurs much easier than homogeneous nucleation. For heterogeneous nucleation, particles prefer to grow on certain sites, for example, grain boundaries, surfaces or impurities. Due to these preferential grow sites, the surface energy

balance of heterogeneous nucleation is much lower and decreases the energy barrier for particle formation (seen below in Fig. 15), which will accelerate the nucleation rate and be favorable to occur.

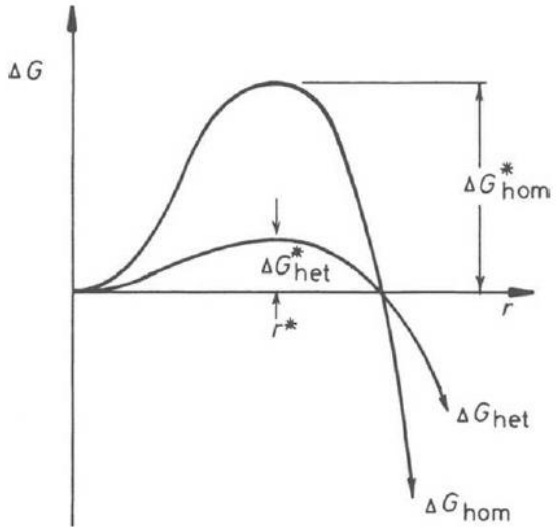

Fig. 15. The free energy barrier of solid phase for homogeneous and heterogeneous nucleation [50]

The Equation of Gibbs free energy change for homogenous nucleation is shown as:

$$\Delta G_{homo} = \frac{4\pi}{3} r^3 \Delta G_v + 4\pi r^2 \gamma_{\alpha\beta} \quad (19)$$

Thus, the Gibbs free energy change depends on both volume free energy (ΔG_v) and interfacial energy ($\gamma_{\alpha\beta}$) factors.

The Equation of free energy for heterogeneous nucleation is shown as:

$$\Delta G_{heter} = \Delta G_{homo} * f(\theta) = \left(\frac{4\pi}{3} r^3 \Delta G_v + 4\pi r^2 \gamma_{\alpha\beta} \right) * f(\theta) \quad (20)$$

where $$f(\theta) = (2 + \cos\theta)(1- \cos\theta)^2 /4 = 2 - 3\cos\theta + \cos^3\theta /4 \quad 0 \le f(\theta) \le 1 \quad (21)$$

In these equations, r is the radius of the nucleus particle and $\gamma_{\alpha\beta}$ is the interfacial tension between two phases. From Equation (19-21), it can be seen $\Delta G_{heter} < \Delta G_{homo}$, which means nucleation barriers is significantly lower and heterogeneous nucleation is

preferred. Further studies are required for a more detailed analysis of these kinetics.

Since $LaMnO_3$ directly attaches to the surface of $LaCrO_3$, the possibility of diffusion needs to be considered. It is possible that the Cr could diffuse and dope into $LaMnO_3$, because $LaMnO_3$ and $LaCrO_3$ perovskites have a similar structure and valence bandwidth. Also, Mn^{3+} in $LaMnO_3$ and Cr^{3+} in $LaCrO_3$ have a similar ionic radius and the location of Mn^{3+} and Cr^{3+} ions are occupied at the same energy level, which means ions would have exchange interaction without any essential difference [56,57]. According to the experiments of Deisenhofer and Zhang et al. [58,59], Cr-doped Lanthanum Manganite, $LaMn_{1-x}Cr_xO_3$, was formed using the standard solid state reaction over 1000 ºC for 120h with rhombohedral structure.

The diffusion time can be calculated by using equations (22) and (23) [60] below,

$$D=D_0*\exp(-Q/RT) \tag{22}$$

$$L(t) = \sqrt{Dt} \tag{23}$$

where D and Q are the diffusion coefficient(m^2/s) and the activation energy(kJ/mol) respectively. R and T represent the gas constant (8.31446 J/(mol*K)) and the absolute temperature(K). L(t) represents the diffusion length as a function of time, t. For example, the diffusion coefficient ($D_{eff\text{-}Mn}$) of Mn in $LaMnO_3$ is approximately $3.25*10^{-11}$ cm^2/s at 1523K when P_{o2} =1bar. The diffusion coefficient ($D_{eff\text{-}Cr}$) of Cr in $LaMnO_3$ is around $5.4*10^{-12}$ cm^2/s in the same conditions, which is one order of magnitude lower than $D_{eff\text{-}Mn}$ [61]. Then the calculated diffusion length of Cr into $LaMnO_3$ is around 0.028nm at 550 ºC for 8h in this study. Therefore, the solid diffusion rate of Cr into the $LaMnO_3$ is very slow

and the formation of $LaMn_{1-x}Cr_xO_3$ should not be an issue under the conditions of this experiment.

This study mainly focuses on various effects of different synthesis conditions on the formation of core-shell particles by the molten salt method. The parameters investigated are: (a) synthesis time which changes the thickness of $LaMnO_3$ shell, (b) $LaCrO_3$-$LaMnO_3$ core-to-shell weight ratio that can influence the amount and shape of core-shell particles formed, (c) size of the $LaCrO_3$ core particle which can influence the total interfacial energy contribution to the nucleation process. The formation of the core materials is described in Chapter 2. Based on the previous results in Chapter 2, this study was performed only with the synthesis temperature of 550 ºC to ensure the formation of the $LaMnO_3$ shell phase.

3.2. Experiments

3.2.1. Molten salt synthesis of $LaCrO_3$-$LaMnO_3$ core-shell particle

3.2.2.1. Synthesis of $LaCrO_3$ - $LaMnO_3$ core-shell particle

The precursor powders (La_2O_3 and Mn_2O_3) used for the shell material are hundreds of nanometer-scale mixtures. The mixture powders were SPEX milled using zirconia milling media for 1h 30min (the reason for SPEX milling will be discussed in 3.3.1). $LaCrO_3$, which was already formed by the molten salt method, was SPEX milled for 5h and then was added to the mixture. After drying in the oven overnight, the mixture was added to the eutectic mixture of LiCl-KCl salts followed by reacting in a box furnace at 550 ºC for 8h. After cooling down and removing from the box furnace, the salts were dissolved in de-ionized water. The powders were washed and dried at 80 ºC in the oven.

3.2.2.2. Characterization

The crystal structure was studied by XRD using a Bruker D8 instrument (Cu-Kα radiation). SEM and STEM images of the particles were obtained to identify the particle microstructure. Energy dispersive x-ray (EDS) element analysis and mapping were used to measure the distribution of different elements in the core ($LaCrO_3$) and shell ($LaMnO_3$) regions by Zeiss Supra55VP Field Emission SEM (FESEM) instrument.

3.2.2. Molten salt synthesis of LSCF-$LaMnO_3$ core-shell particle

3.2.2.1. Synthesis of LSCF - $LaMnO_3$ core-shell particle

The mixture of La_2O_3, Mn_2O_3 and LSCF powders were all SPEX milled together for 1h 30min using zirconia milling media and dried overnight at 80 ºC. LiCl-KCl salts were added into the crucible with the mixture of precursor powders and then it was heated in the box furnace at 500 ºC for 8h. After the reaction, the salts were dissolved as before and the powders remaining in the crucible were dried at 80 ºC.

3.2.2.2. Characterization

As before XRD patterns were obtained using Cu-Kα radiation (Bruker D8 instrument). The microstructure was examined by SEM and STEM.

3.3. Results and Discussions

3.3.1. $LaCrO_3$-$LaMnO_3$ core-shell particle

In the first attempt, La_2O_3, Mn_2O_3 and $LaCrO_3$ powders were stirred roughly by hand and thus they were not uniformly mixed before the molten salt reaction. These unmixed powders were directly heated in the box furnace. The SEM image (Fig. 16) shows

that there are large agglomerates which are rich in Cr (Region 2 in Table 3) and that other regions barely contain Cr (Region 1 in Table 3). So it is obvious that $LaCrO_3$ aggregated and $LaMnO_3$ didn't attach on $LaCrO_3$ surface. This indicates that well mixing before the molten salt reaction is necessary.

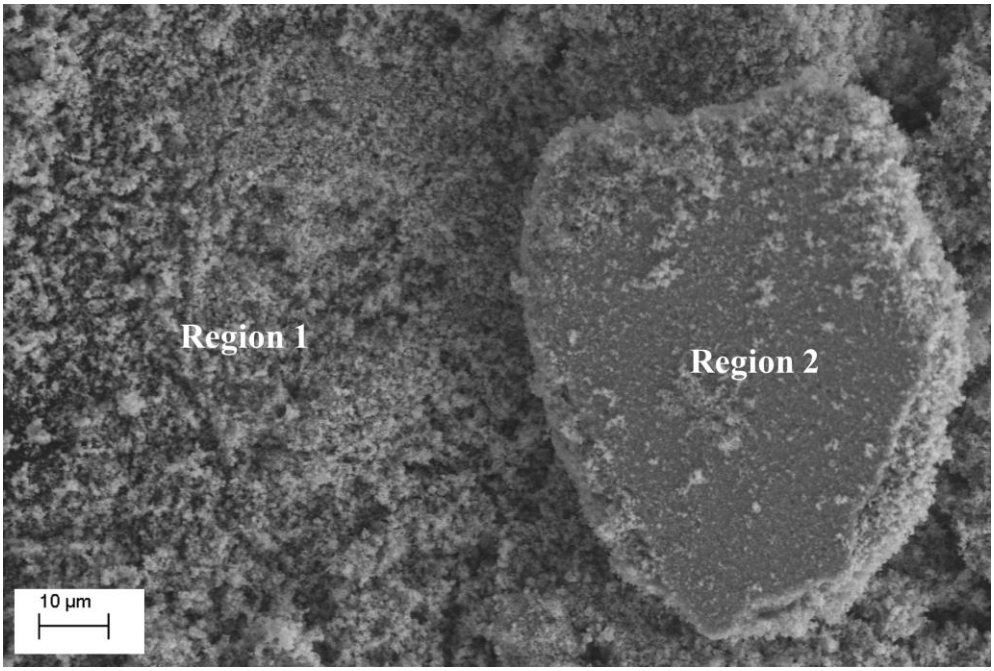

Fig. 16. SEM image of agglomerated $LaCrO_3$ and $LaMnO_3$

Element	La	O	Mn	Cr
Region 1	25.33	53.60	19.74	1.33
Region 2	38.05	26.62	6.11	29.22

Table 3. The composition distribution (atomic %) of different regions selected in SEM image Fig.16

The successful synthesis of the core-shell structures may also depend on the particle size of the $LaCrO_3$ core. In this study, the effect of core size was studied by introducing SPEX milling of the core particles, as shown in Fig. 17. The core size without SPEX

milling was ~ 1.5μm. After SPEX milling in ethanol for 5h, the size reduced to the nanometric scale around 500nm.

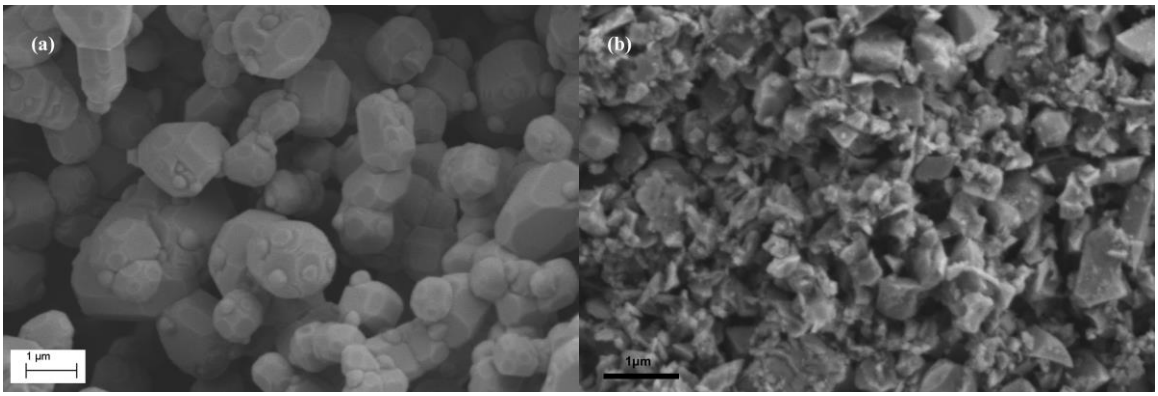

Fig. 17. SEM images of $LaCrO_3$ particles at different size: (a) No SPEX milling (b) SPEX milling for 5h

$LaCrO_3$ particles with and without SPEX milling were used to synthesize the core-shell structure under otherwise identical reaction conditions. Fig. 18 (a) shows the results using the particles without SPEX milling. The particles within the red circle are a segregated $LaCrO_3$ phase after the reaction. This indicates that the intended $LaMnO_3$ shell particles could not attach to the $LaCrO_3$ surface. However, a core-shell cubic structure appears to be formed after decreasing the size of the $LaCrO_3$ (Fig. 18 (b)), i.e. the SPEX-milled core particles. This indicates that smaller core size is preferred.

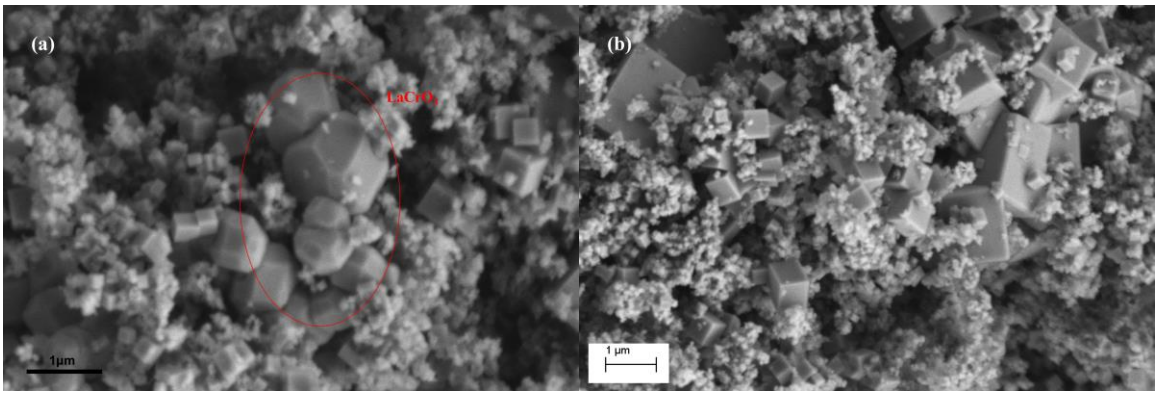

Fig. 18. SEM images of core-shell particles at different $LaCrO_3$ core size: (a) No SPEX milling (b) SPEX milling for 5h

Segregation into two phases with non-uniform microstructure and different sizes points at the importance of the mixing by SPEX milling step in the core-shell preparation process. The SPEX milling reduces the core particle size providing more sites for heterogeneous nucleation. Therefore, in order to synthesize $LaCrO_3$-$LaMnO_3$ core-shell structure successfully, the $LaCrO_3$ core was SPEX milled for 5h during the preparation process to decrease the size. Additionally, La_2O_3, Mn_2O_3 and $LaCrO_3$ mixtures were further blended and SPEX milled for 2h to break the agglomeration in all following experiments.

XRD patterns were obtained for the powder formed using the SPEX milled $LaCrO_3$ and the results are shown in Fig. 19. All the diffraction peaks in the XRD pattern are indexed to cubic $LaMnO_3$ peaks with no longer any more precursors. This means $LaMnO_3$ successfully formed around the $LaCrO_3$ particles at 550 ºC synthesis temperature.

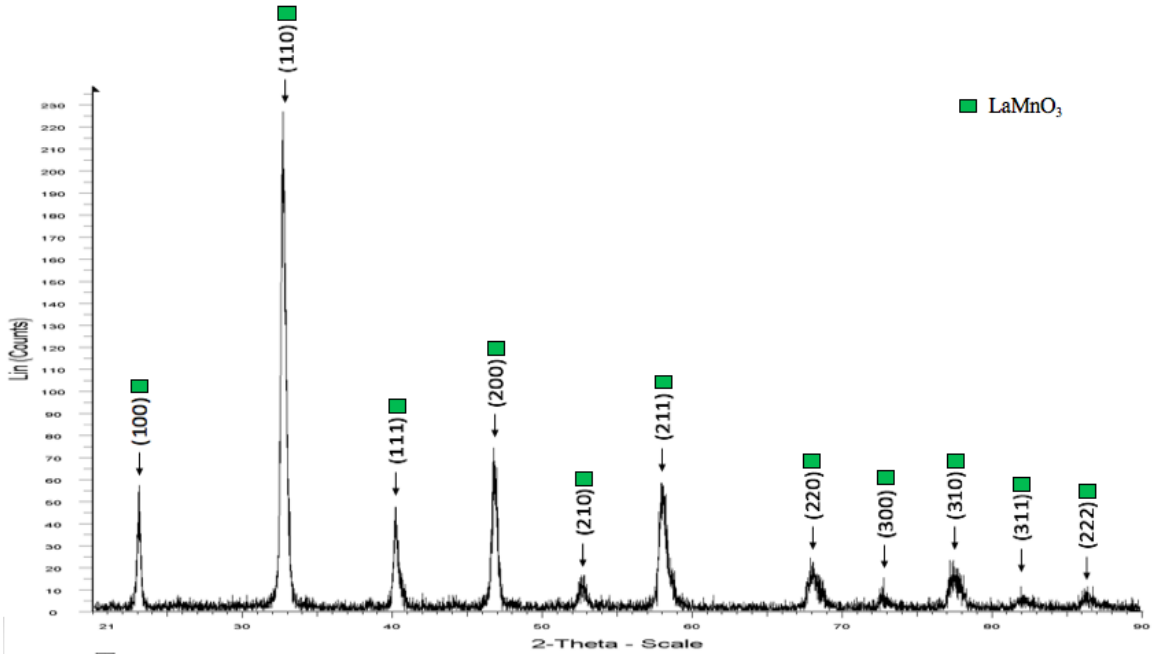

Fig. 19. X-ray diffraction pattern of particles with weight ratio $LaMnO_3$: $LaCrO_3$= 3:0.5

The resulting $LaCrO_3$-$LaMnO_3$ particles were also analyzed by EDS using the SEM and the results are detailed in Table 4. Measurements were obtained on selected spots within the particles (one in the center of the particle and another one on the edge). Based on EDS analysis of four different particles, the conclusions are consistent, i.e. the core-shell structure has been successfully synthesized. Based on the EDS analysis, it is evident that the Mn to Cr ratio is lower in the core region and Mn to Cr ratio is higher in the shell region implying a $LaCrO_3$ -rich the core, and $LaMnO_3$ – rich shell.

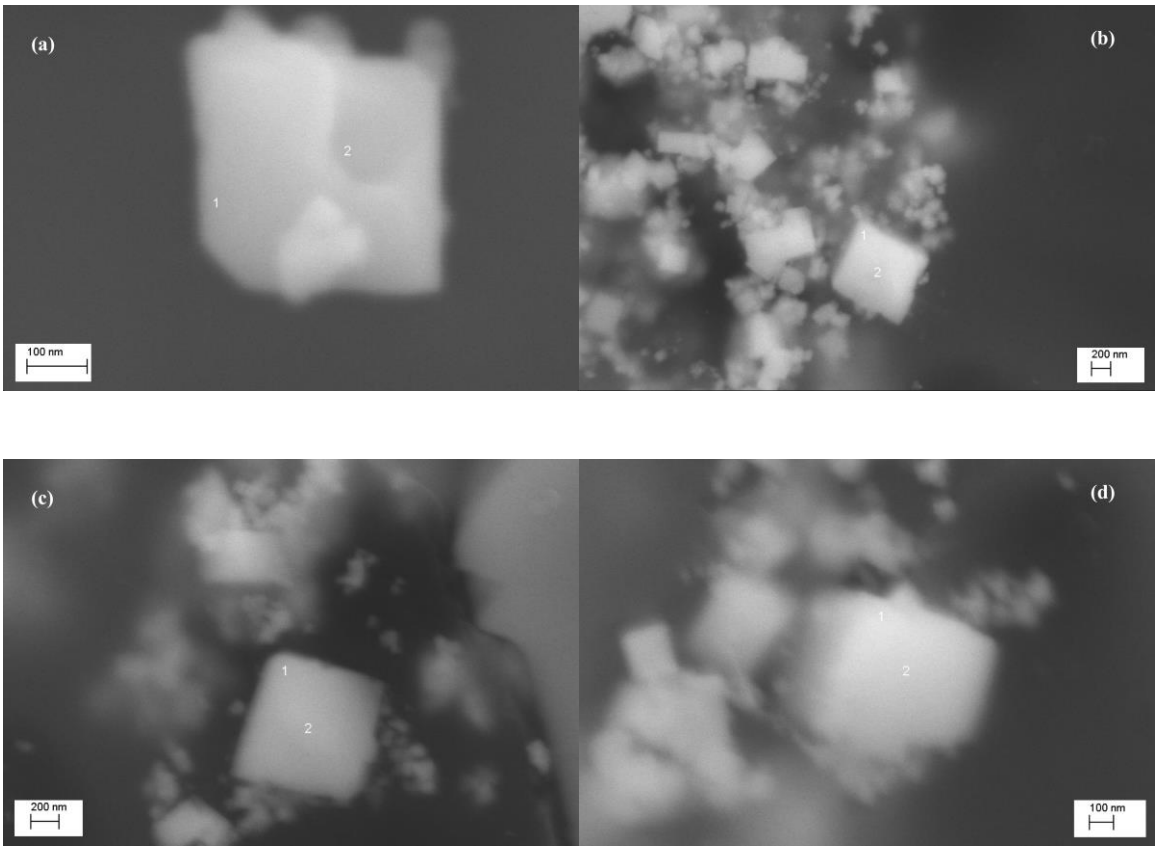

Fig. 20. SEM images of particles determined by EDS at various spots with weight ratio $LaMnO_3$: $LaCrO_3$= 3:0.5

Element	La	O	Mn	Cr	Mn : Cr
Spot (a)1	17.01	67.24	12.11	3.64	3.3269:1
Spot (a)2	16.20	68.34	9.98	5.48	1.8212:1
Spot (b)1	22.70	57.60	17.03	2.68	6.3544:1
Spot (b)2	19.15	64.00	8.50	8.35	1.0179:1
Spot (c)1	19.71	58.94	20.13	1.23	16.3659:1
Spot (c)2	18.63	64.03	12.54	4.80	2.6125:1
Spot (d)1	16.30	69.22	13.27	1.21	10.9669:1
Spot (d)2	17.98	66.14	12.06	3.82	3.1571:1

Table 4. The composition distribution (atomic %) of $LaCrO_3$-$LaMnO_3$ core-shell particle with weight ratio $LaMnO_3$: $LaCrO_3$= 3:0.5 (Note: spot 1 is in the edge and spot 2 is in the center of particle)

These EDS results measured at different spots provides more experimental evidence to support the formation of core-shell structure.

The diameter of EDS electron beam is around 50nm. However, the incident EDS e-beam may have the interaction with the sample and is scattered in the sample, as shown in the blue area in Fig. 21. The scattering range of EDS e-beam is much larger than the size of particles, but the particles still can be measured due to its small thickness, which is beyond the range of the beam start to scatter. Besides, further measurements by using Transmission electron microscopy (TEM) may be needed for better understanding and more demonstration.

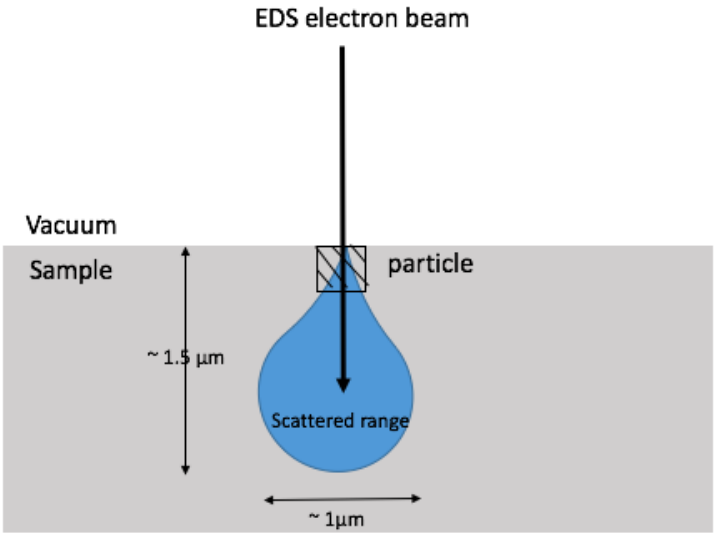

Fig. 21. Primary EDS electron beam-sample interactions

In Fig. 22 and Fig. 23, SEM and STEM images show the uniform cubic structure of core-shell particles. The size of particles was distributed randomly. This result can be explained as the uneven thermal equilibrium in the molten salt circumstance at the different places since stirring is not involved during the reaction. Powders reacted at different spots

with different temperatures, which caused the growth of particles at different rates.

After preparing the core-shell type particles successfully, synthesis time and core to shell weight ratio were studied holding the core size and reaction temperature constant. It was found that this significantly influenced the microstructure and shell thickness of the particle.

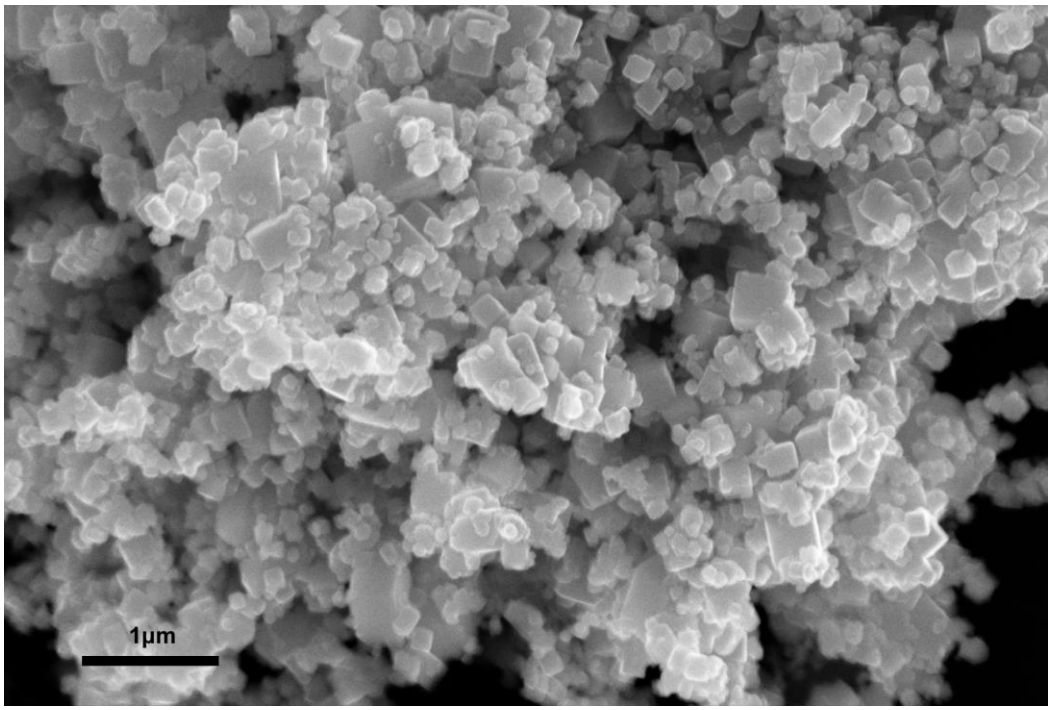

Fig. 22. SEM image of core-shell particle with weight ratio $LaMnO_3$: $LaCrO_3$= 3:0.5

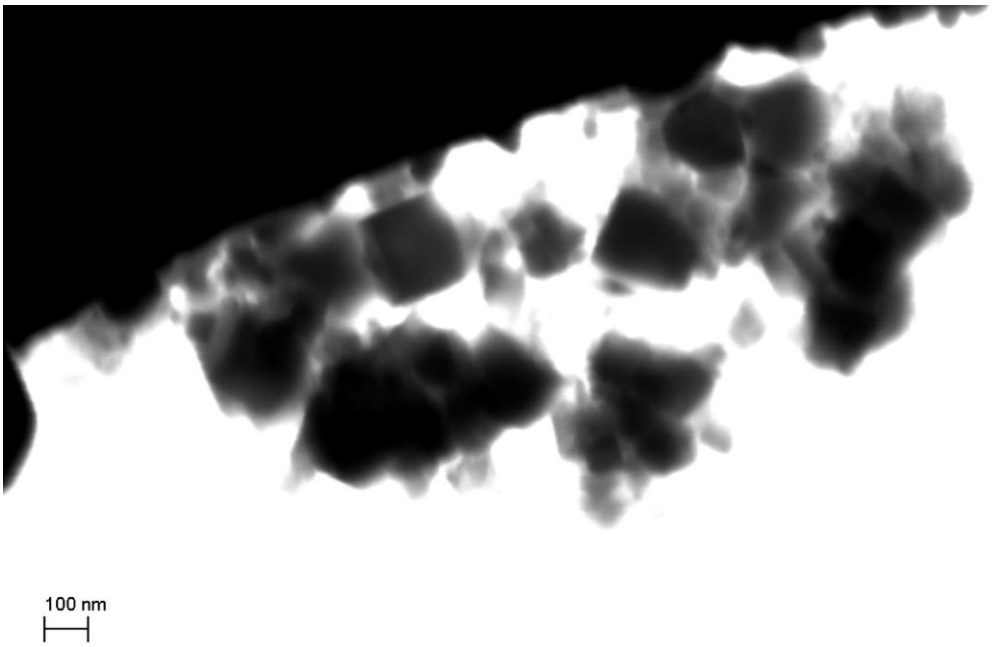

Fig. 23. STEM image of core-shell particle with weight ratio $LaMnO_3$: $LaCrO_3$= 3:0.5

The XRD patterns obtained from reacted mixtures containing various targeted weight ratios of $LaMnO_3$: $LaCrO_3$ (3 : 0.5 , 3 : 1 , 1 : 1 , 1 : 3) are shown in Fig.24. They all show the characteristic $LaMnO_3$ perovskite peaks with small amounts of LaOCl when the weight ratio is 1:3. This secondary phase was expected from prior experiments as an intermediate phase and is already discussed in Chapter 2.

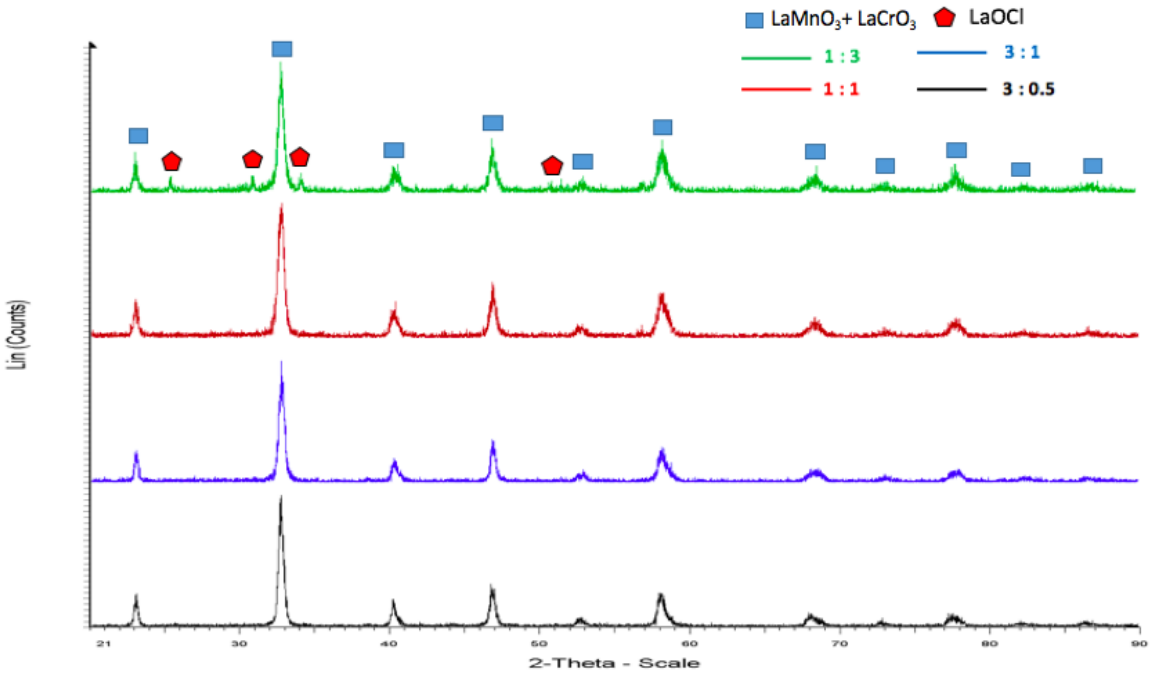

Fig. 24. X-ray Diffraction patterns of core-shell particles at different weight ratio ($LaMnO_3$: $LaCrO_3$): (a) 3 : 0.5 ; (b) 3 : 1 ; (c) 1 : 1 ; (d) 1 : 3

The weight ratio of the core ($LaCrO_3$) and shell ($LaMnO_3$) can affect the amount and shape of core-shell particles as well. When the weight ratios ($LaMnO_3$: $LaCrO_3$) were 3:0.5 and 3:1, as shown in Fig. 25(a)(b), the particles were all formed in a cubic shape. However, in Fig. 25 (c) (d), by increasing the weight ratio of core particles to reach 1:1 and 1:3, the amount of cubic shape particles is greatly reduced and nearly cannot be found. The shape of synthesized particles is spherical rather than cubic. This may because the thickness of shell become smaller and spherical core particles are surrounded by a thin shell.

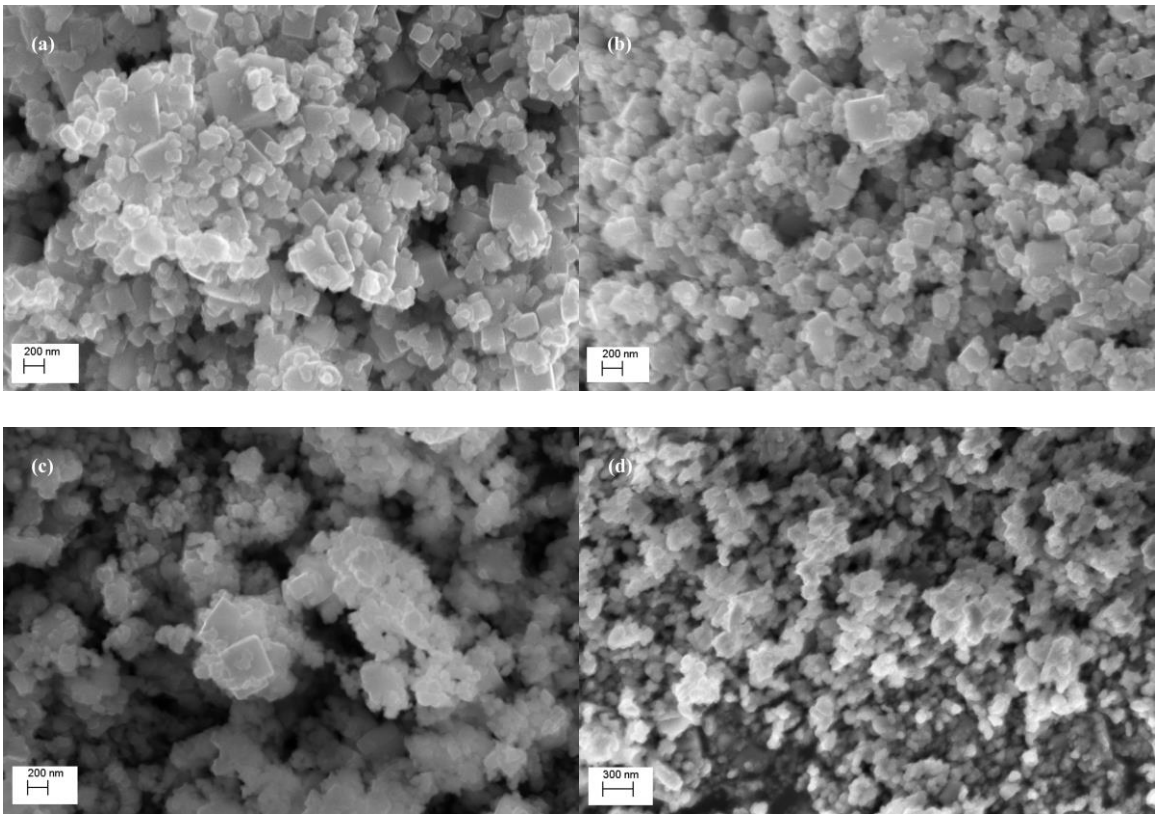

Fig. 25. SEM images of core-shell particles at different weight ratio ($LaMnO_3$: $LaCrO_3$): (a) 3 : 0.5 (b) 3 : 1 (c) 1 : 1 (d) 1 : 3

EDS elemental analysis was done at weight ratio of 3:1 and 1:1 to confirm the core-shell structure was synthesized, as shown in Table 5 and 6. However, particles with cubic shape could not be found at the ratio of 1:3 and the particles are all aggregated. Therefore, EDS was not used on 1:3 ratio sample.

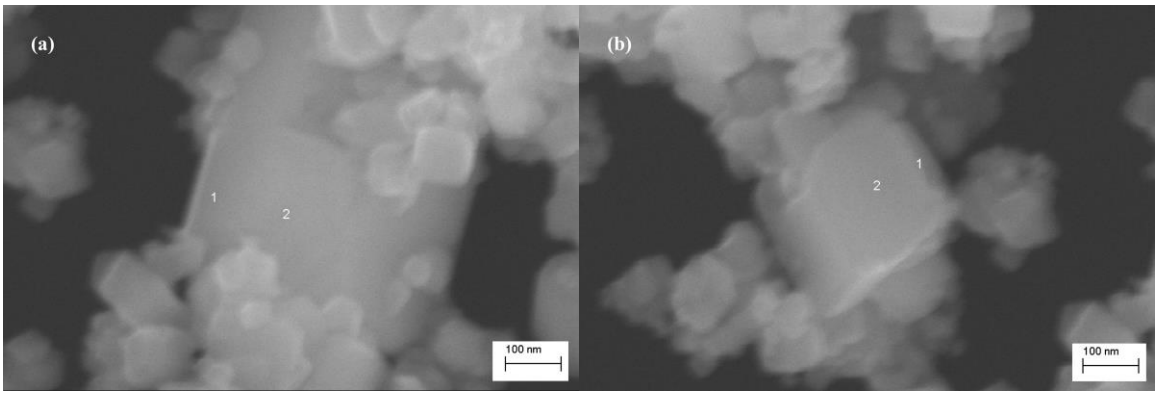

Fig. 26. SEM images of particles determined by EDS at various spots with weight ratio $LaMnO_3$: $LaCrO_3$= 3:1

Element	La	O	Mn	Cr	Mn : Cr
Spot (a)1	9.04	81.17	8.16	1.63	5.0061:1
Spot (a)2	10.27	78.89	7.79	3.06	2.5458:1
Spot (b)1	9.74	79.98	7.28	2.99	6.3544:1
Spot (b)2	9.32	81.55	5.09	8.35	1.0179:1

Table 5. The composition distribution (atomic %) of $LaCrO_3$-$LaMnO_3$ core-shell particle with weight ratio $LaMnO_3$: $LaCrO_3$= 3:1

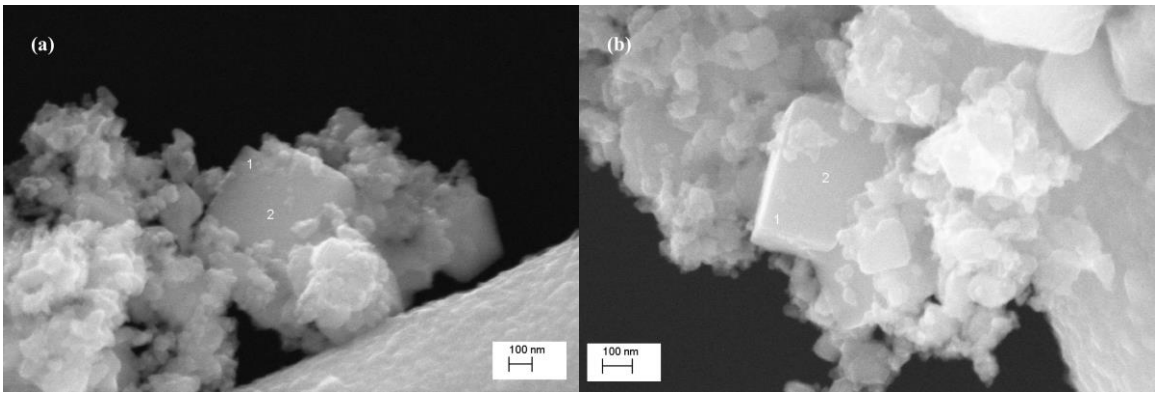

Fig. 27. SEM images of particles determined by EDS at various spots with weight ratio $LaMnO_3$: $LaCrO_3$= 1:1

Element	La	O	Mn	Cr	Mn : Cr
Spot (a)1	17.78	63.37	14.88	3.97	3.7481:1
Spot (a)2	21.45	56.98	12.83	8.75	1.4663:1
Spot (b)1	9.61	80.72	6.81	2.86	2.3811:1
Spot (b)2	11.14	77.57	7.05	4.24	1.6627:1

Table 6. The composition distribution (atomic %) of $LaCrO_3$-$LaMnO_3$ core-shell particle with weight ratio $LaMnO_3$: $LaCrO_3$= 1:1

The reaction time can also affect the core-shell particle size. XRD and SEM results (Fig. 28 and Fig. 29 (a) (b)) showed no difference in the $LaMnO_3$ peaks when the reaction time changed at the same compositional ratio and synthesis temperature ($LaMnO_3$: $LaCrO_3$ = 3:0.5). However, when the reaction happened in very short time, there was byproduct LaOCl forming with core-shell particle. EDS measurements (Fig. 30 (a)(b)) at different spots were done to confirm the formation of core-shell structure, as shown in Table 7. This result proves that core-shell structure can be formed even at a very short time for 10min.

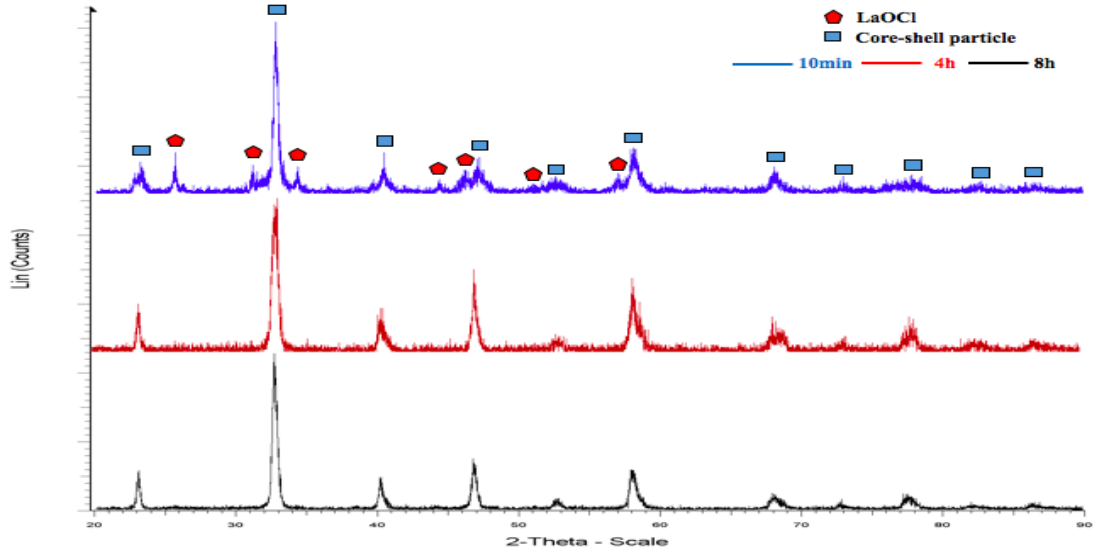

Fig. 28. X-ray Diffraction patterns of core-shell particles at different reaction time ($LaMnO_3$: $LaCrO_3$= 3: 0.5) : 10min; 4 h ; 8 h

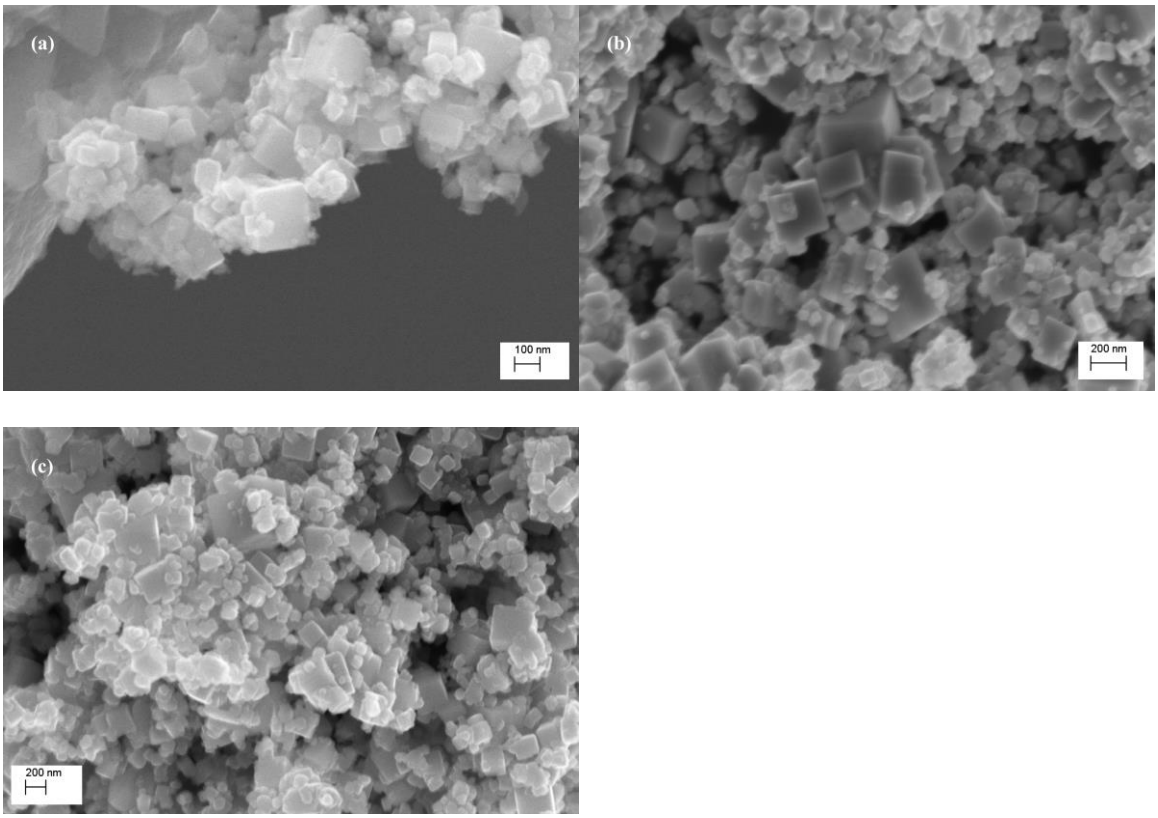

Fig. 29. SEM images of core-shell particles at different reaction time ($LaMnO_3$: $LaCrO_3$= 3: 0.5) : 10min; 4 h ; 8 h

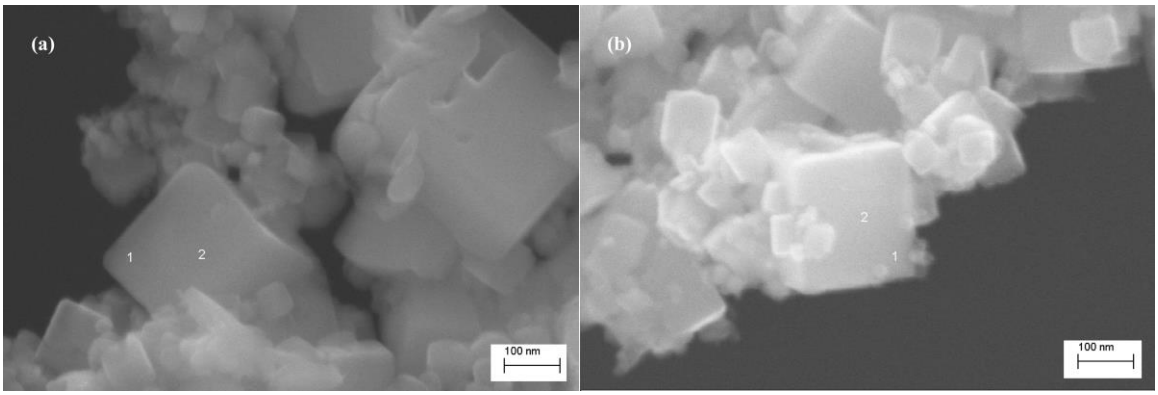

Fig. 30. SEM images of particles determined by EDS at various spots with weight ratio $LaMnO_3$: $LaCrO_3$= 3:0.5 for 10min

Element	La	O	Mn	Cr	Mn : Cr
Spot (a)1	8.55	81.70	9.17	0.58	15.8103:1
Spot (a)2	8.51	80.61	9.62	1.26	7.6349:1
Spot (b)1	8.86	81.12	8.97	1.05	8.5429:1
Spot (b)2	9.53	79.10	9.32	2.05	4.5463:1

Table 7. The composition distribution (atomic %) of $LaCrO_3$-$LaMnO_3$ core-shell particle with weight ratio $LaMnO_3$: $LaCrO_3$= 3:0.5 for 10min

3.3.2. LSCF-$LaMnO_3$ core-shell particle

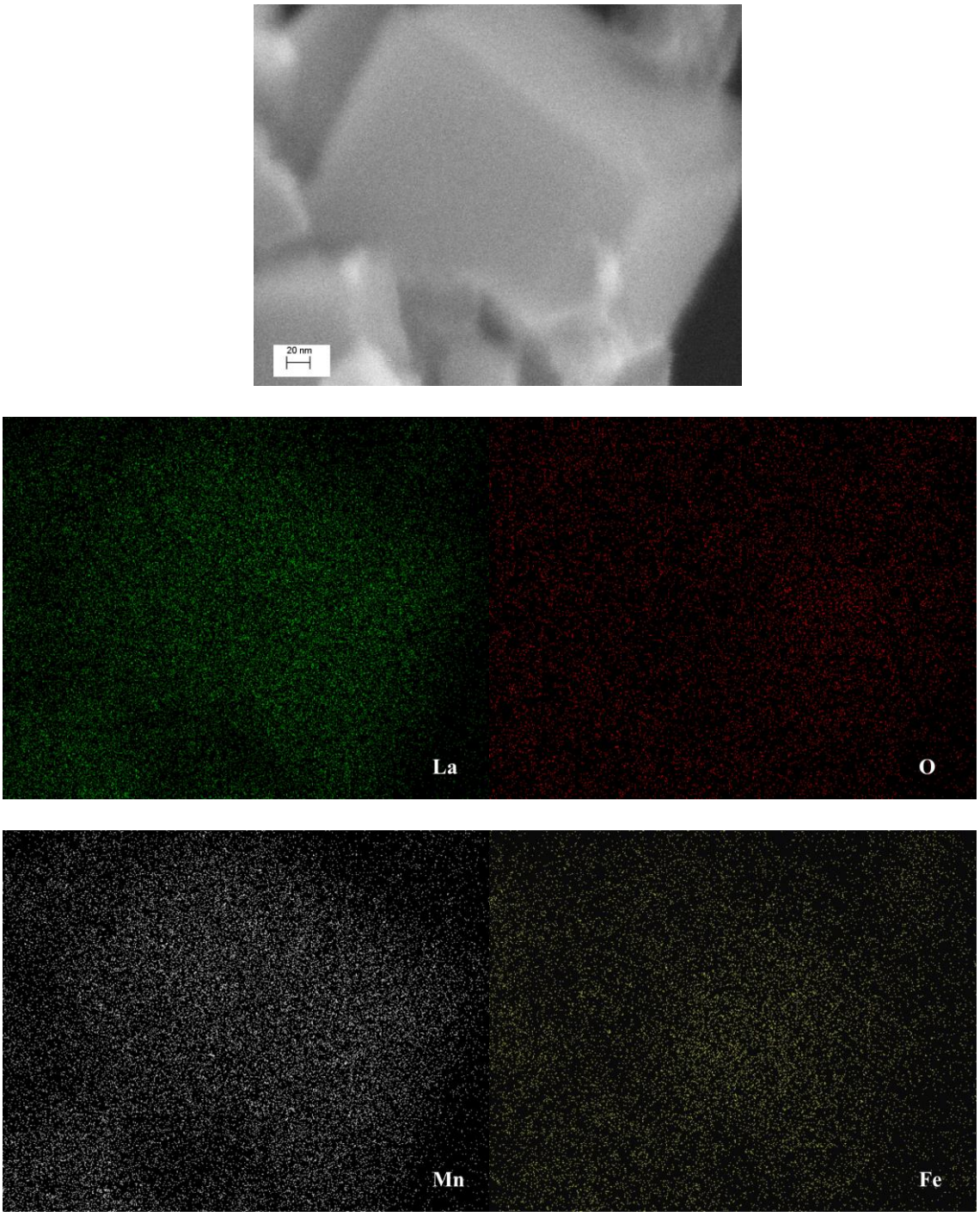

Fig. 31. Elemental mapping analysis on LSCF-$LaMnO_3$ particle by EDS. As indicated on the image: Green for La, Red for O, Grey for Mn, and Yellow for Fe.

This study uses EDS elemental analysis and mapping to confirm the formation of LSCF-$LaMnO_3$ core-shell structure. In Fig. 31, the distribution of different elements on LSCF-$LaMnO_3$ core-shell particles is presented. The grey areas indicate the presence of greater amounts of Mn in the shell region. The yellow areas show Fe element are segregated in the middle (core) region. La and O elements are distributed uniformly on the particles. EDS elemental mapping clearly indicates that molten salt method effectively forms core-shell type particles.

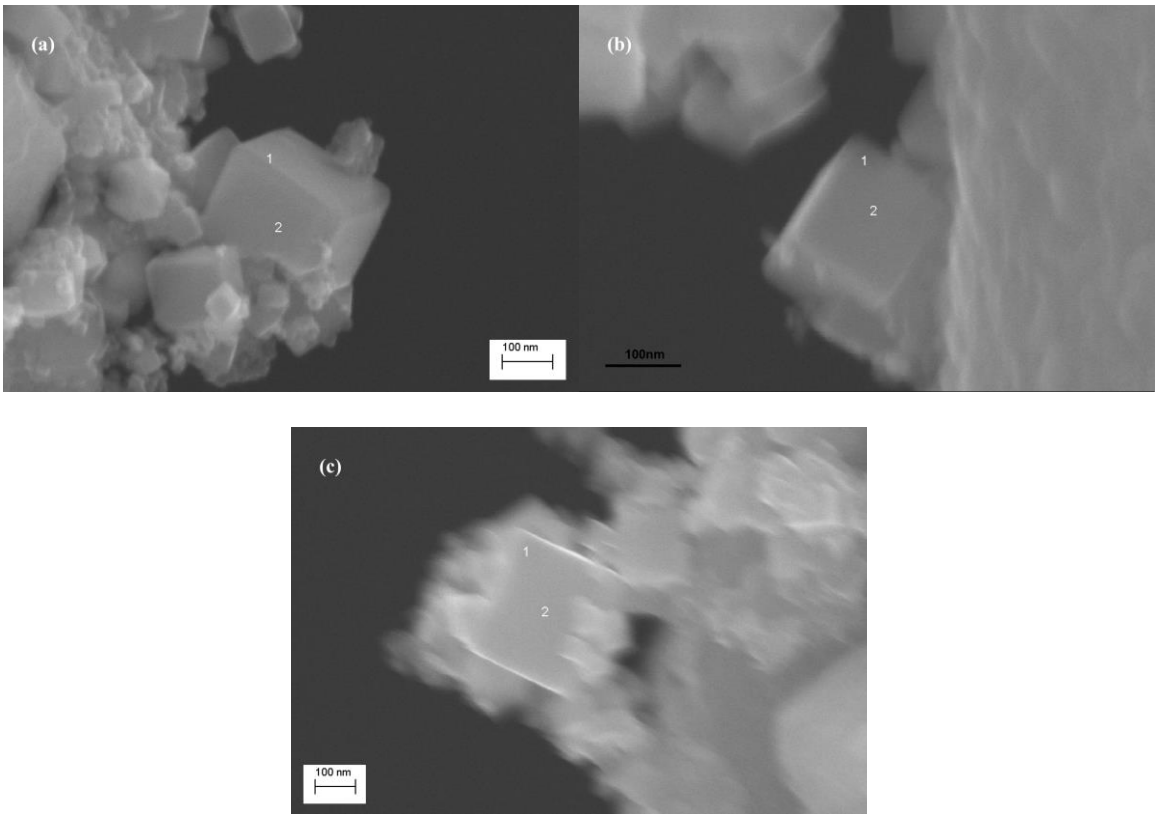

Fig. 32. SEM images of particles determined by EDS at various spots with weight ratio $LaMnO_3$: LSCF= 3:0.5

Table 8 summarizes the EDS elemental analysis results of the composition distribution (atomic %) of LSCF-$LaMnO_3$ synthesized core-shell particles at selected

spots. It further shows the core-shell structure has been successfully formed. It is seen that the composition distribution of Mn to Fe ratio is lower in the core region and higher in the shell region, implying that LSCF is more concentrated in the core region.

Element	La	O	Mn	Fe	Co	Mn : Fe
Spot (a)1	22.33	43.75	27.20	5.69	1.04	4.7803:1
Spot (a)2	24.33	36.60	24.90	12.03	2.14	2.0698:1
Spot (b)1	9.55	79.28	9.23	1.48	0.46	6.2364:1
Spot (b)2	9.83	78.71	8.87	2.05	0.54	4.3268:1
Spot (c)1	7.46	82.37	8.55	1.15	0.46	7.4348:1
Spot (c)2	8.65	80.09	8.00	2.64	0.62	3.0303:1

Table 8. The composition distribution (atomic %) of LSCF-$LaMnO_3$ core-shell particle with weight ratio $LaMnO_3$: LSCF= 3:0.5

SEM and STEM images of synthesized LSCF-$LaMnO_3$ core-shell particles are shown in Fig. 33 and Fig. 34. The size of the particles ranges from 100 to 400 nm.

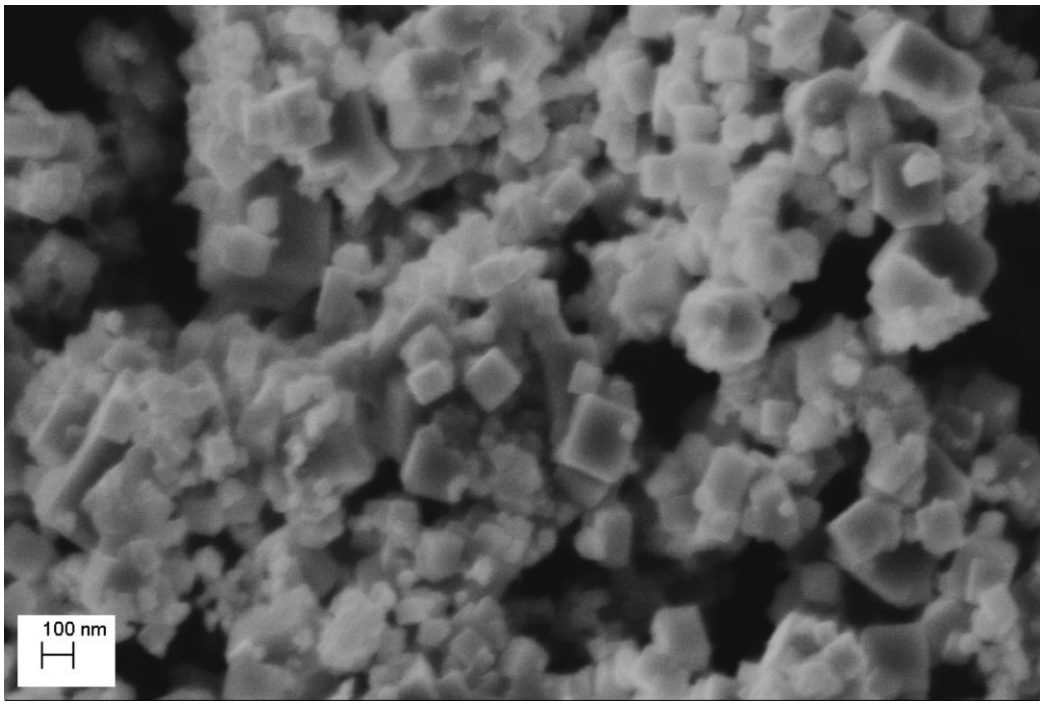

Fig. 33. SEM image of core-shell particle with weight ratio $LaMnO_3$: LSCF = 3:0.5

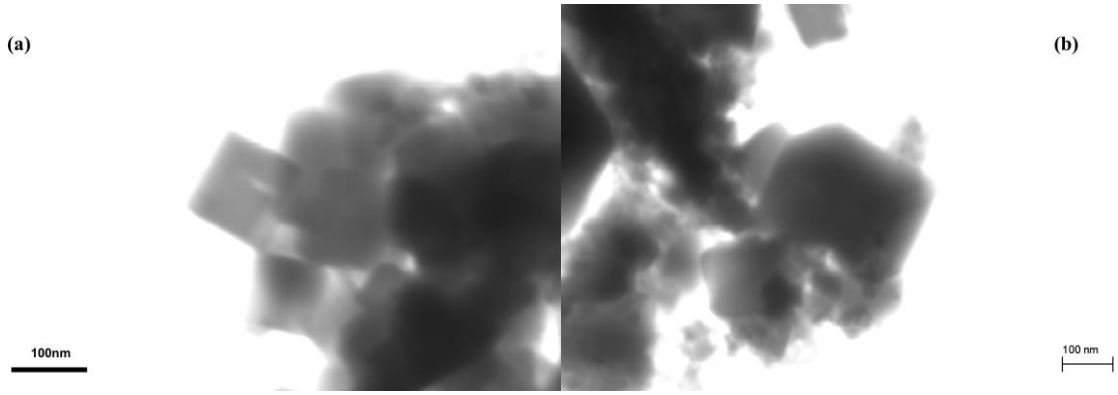

Fig. 34. STEM images of core-shell particle with weight ratio $LaMnO_3$: LSCF = 3:0.5

As in Section 3.3.1 for $LaCrO_3$-$LaMnO_3$ core-shell particles, this section also discusses the effects of core-shell weight ratio without changing core size and reaction time. There is no noticeable change in the XRD patterns as shown in Fig.35 and have the

similar microstructures in the SEM as shown in Fig. 36 when the weight ratio of $LaMnO_3$: LSCF is 3 : 0.5 and 3:1 respectively.

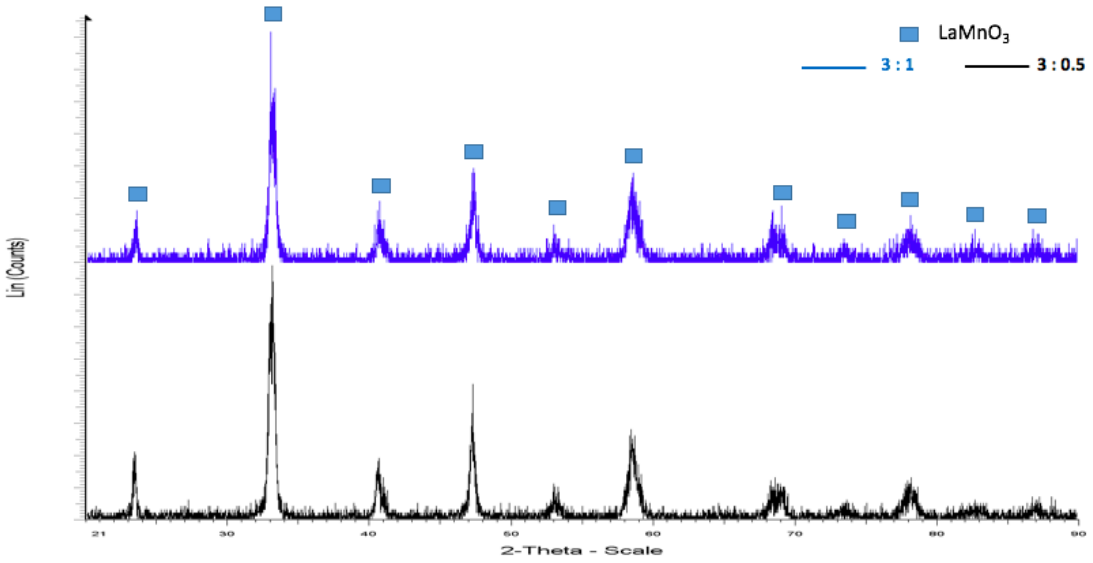

Fig. 35. X-ray Diffraction patterns of core-shell particles at different weight ratio ($LaMnO_3$: LSCF): 3 : 0.5 ; 3 : 1

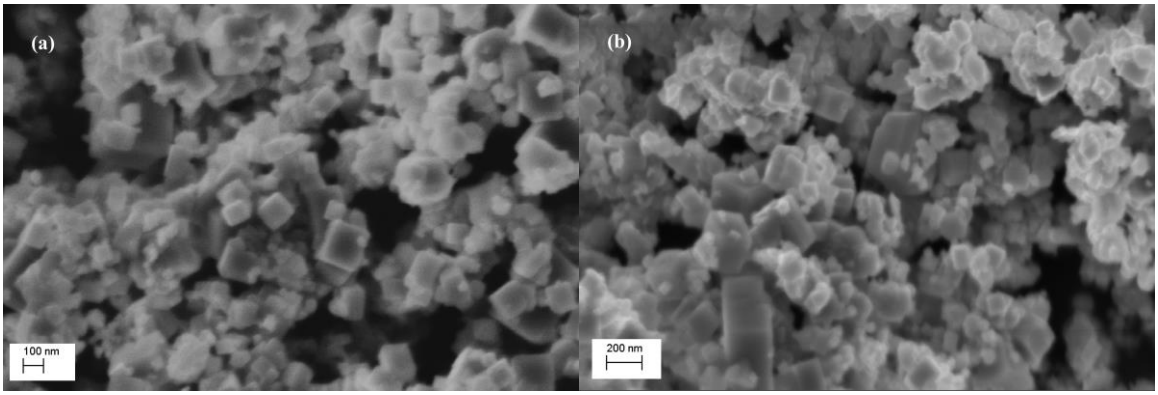

Fig. 36. SEM images of core-shell particles at different weight ratio ($LaMnO_3$: LSCF): (a) 3 : 0.5 (b) 3 : 1

3.4. Conclusions

The successful formation of the core-shell structure through the molten salt method shows the preferential heterogeneous growth of the $LaMnO_3$ shell on the core particles ($LaCrO_3$ and LSCF). The size of $LaCrO_3$ and LSCF core, and the weight ratio of the core to shell material plays an important role in determining the microstructure of the product. However, it appears that reaction time may not make any difference so long as it is sufficiently long to ensure the complete formation of the shell region.

4. CONCLUSIONS

Previous work has mostly focused on solid state reaction at high temperature or the combustion method to synthesis $LaCrO_3$, $LaMnO_3$ and LSCF particles. These synthesis methods are all costly and time-consuming. This study demonstrates that nanoscale $LaCrO_3$, $LaMnO_3$ and LSCF perovskites can be easily formed by molten salt synthesis in the LiCl-KCl salt system at much lower temperatures (400 ºC – 550 ºC). The energy usage and reaction times during materials synthesis can be greatly reduced through the molten salt method. Moreover, the precursors used are inexpensive and the size and compositions of the particles are easy to control. Then the molten salt method was also used to form core-shell structured particles such as $LaCrO_3$-$LaMnO_3$ and LSCF-$LaMnO_3$ at 550 ºC. The EDS results suggest the successful formation of expected $LaCrO_3$-$LaMnO_3$ and LSCF-$LaMnO_3$ core-shell particles with a cubic symmetry. Based on these results, we conclude that molten salt synthesis method is an attractive alternative route for the synthesis of complex transition metal perovskites and core-shell structures based on such transition metal perovskites.

5. SUGGESTIONS FOR FUTURE WORK

This work shows proof of concept of the successful formation of $LaCrO_3$, $LaMnO_3$ and LSCF through the molten salt method and its use to synthesize core-shell structures. It is still necessary to investigate much shorter times during the synthesis as a means to control shell thickness and its effect on the electrical conductivity and oxygen exchange kinetics of SOFC cathodes constructed out of such core-shell materials. The effect of the core to shell thickness ratios should also be investigated. Further, Transmission electron microscopy (TEM) should be used to image the core-shell structure and to understand the orientation relationships in the core-shell structure.

Besides, more works can be done involving different kinds of core and shell materials or different kinds of shapes. For example, $LaCrO_3$ doped with alkaline earth metals can be investigated. Thus molten salt synthesis of core-shell particles can be expanded to form various kinds of core-shell structure particles.

BIBLIOGRAPHY

1. US Department of Energy. Comparison of Fuel Cell Technologies. Energy Efficiency and Renewable Energy (2016). at <http://energy.gov/eere/fuelcells/comparison-fuel-cell-technologies>

2. Hernández, E., V. Sagredo, and G. E. Delgado. "Synthesis and magnetic characterization of $LaMnO_3$ nanoparticles." Revista Mexicana de Física **61.3** (2015): 166–169.

3. Gawande, Manoj B., et al. "Core–shell nanoparticles: synthesis and applications in catalysis and electrocatalysis." Chemical Society Reviews **44.21** (2015): 7540–7590.

4. Ghosh Chaudhuri, Rajib, and Santanu Paria. "Core/shell nanoparticles: classes, properties, synthesis mechanisms, characterization, and applications." Chemical Reviews **112.4** (2011): 2373–2433.

5. Arfsten, Nanning Joerg, et al. "Core-shell nanoparticles." U.S. Patent Application No. 12/438,596.

6. Liu, Xiaofeng, Nina Fechler, and Markus Antonietti. "Salt melt synthesis of ceramics, semiconductors and carbon nanostructures." Chemical Society Reviews **42.21** (2013): 8237–8265.

7. Gupta, Sapna, Manoj K. Mahapatra, and Prabhakar Singh. "Phase transformation, thermal expansion and electrical conductivity of lanthanum chromite." Materials Research Bulletin **48.9** (2013): 3262–3267.

8. Tiwari, Brajesh, et al. "Magnetostructural and magnetocaloric properties of bulk $LaCrO_3$ system." Materials Research Express **2.2** (2015): 026103.

9. Khetre, S. M., H. V. Jadhav, and S. R. Bamane. "Synthesis and characterization of nanocrystalline $LaCrO_3$ by combustion route." Rasayan Journal of Chemistry **2** (2009): 174–178.

10. Park, Hong Kyu, et al. "Synthesis of $LaCrO_3$ powders by microwave induced combustion of metal nitrate-urea mixture solution." Journal of Materials Science Letters **17.9** (1998): 785–787.

11. Chick, Larry A., et al. "Glycine-nitrate combustion synthesis of oxide ceramic powders." Materials Letters **10.1–2** (1990): 6–12.

12. Zhigalkina, I. A., et al. "Synthesis of lanthanum chromite using the sol-gel method." Glass and Ceramics **55.5** (1998): 182–185.

13. Zheng, Wenjun, et al. "Hydrothermal synthesis and characterization of $LaCrO_3$." Journal of Materials Chemistry **9.11** (1999): 2833–2836.

14. Kang, Minkyung, et al. "Syntheses of Doped-$LaCrO_3$ Nanopowders by Hydrothermal Method." Open Journal of Inorganic Non-metallic Materials **3.3** (2013): 27.

15. Ding, Xifeng, et al. "Synthesis and characterization of doped $LaCrO_3$ perovskite prepared by EDTA–citrate complexing method." Journal of Alloys and Compounds **458.1** (2008): 346–350.

16. da Conceicao, Leandro, et al. "Combustion synthesis of $La_{0.7}Sr_{0.3}Co_{0.5}Fe_{0.5}O_3$ (LSCF) porous materials for application as cathode in IT-SOFC." Materials Research Bulletin **46.2** (2011): 308–314.

17. Akashi, Takaya, et al. "Solid-State Reaction Kinetics of $LaCrO_3$ from the Oxides and Determination of La^{3+} Diffusion Coefficient." Journal of The Electrochemical Society **145.6** (1998): 2090–2094.

18. Laidler, Keith JKJ. Chemical kinetics. No. 544.4 LAI. 1987.

19. Palcut, Marián, Kjell Wiik, and Tor Grande. "Cation self-diffusion and nonstoichiometry of lanthanum manganite studied by diffusion couple measurements." The Journal of Physical Chemistry C **111.2** (2007): 813–822.

20. Lantelme, Frederic, and Henri Groult. Molten salts chemistry: from lab to applications. Elsevier Amsterdam, 2013.

21. Kimura, Toshio. "Molten salt synthesis of ceramic powders." Advances in Ceramics-Synthesis and Characterization, Processing and Specific Applications. InTech, 2011.

22. Lupis, Claude HP. "Chemical thermodynamics of materials." Elsevier Science Publishing Co., Inc., 1983: 581.

23. Gunawan, Arwin. Thermodynamic considerations in molten salt electrolysis for rare earth metals. Dissertation, Montana Tech of The University of Montana, 2015.

24. Zhang, Qiwu, Jinfeng Lu, and Fumio Saito. "Mechanochemical synthesis of $LaCrO_3$ by grinding constituent oxides." Powder Technology **122.2** (2002): 145–149.

25. Matei, C., et al. "Lanthanum-based perovskites obtained in molten nitrates or nitrites." Progress in Solid State Chemistry **35.2** (2007): 203–209.

26. Guo, Xiaoling, et al. "Semiempirical model for the solubility of rare earth oxides in molten fluorides." Industrial & Engineering Chemistry Research **55.16** (2016): 4773–4781.

27. Ambrová, M., et al. "On the solubility of lanthanum oxide in molten alkali fluorides." Journal of Thermal Analysis and Calorimetry **91.2** (2008): 569–573.

28. Jang, Poknam, et al. "Preparation of Al-La master alloy by thermite reaction in NaF-NaCl-KCl molten salt." JOM **67.5** (2015): 1130–1136.

29. Cherginets, V. L., and E. G. Khailova. "On the solubilities of bivalent metal oxides in molten alkaline chlorides." Electrochimica Acta **39.6** (1994): 823–829.

30. Ishitsuka, Tetsuo, and Koichi Nose. "Stability of protective oxide films in waste incineration environment—solubility measurement of oxides in molten chlorides." Corrosion Science **44.2** (2002): 247–263.

31. Meyer, Joseph Freeman. Recovery boiler superheater corrosion-solubility of metal oxides in molten salt. Dissertation, Georgia Institute of Technology, 2013.

32. Romero, M., et al. "Synthesis by molten salt method of the $AFeO_3$ system (A= La, Gd) and its structural, vibrational and internal hyperfine magnetic field characterization." Physica B: Condensed Matter **443** (2014): 90–94.

33. Srikanth Gopalan, Karun Mehta, and Anil V. Virkar. "Synthesis of oxide perovskite solid solutions using the molten salt method." Journal of Materials Research **11.8** (1996): 1863–1865.

34. Li, Zushu, Shaowei Zhang, and William Edward Lee. "Molten salt synthesis of $LaAlO_3$ powder at low temperatures." Journal of the European Ceramic Society **27.10** (2007): 3201–3205.

35. Huang, Zhong, et al. "Molten salt synthesis of $La_2Zr_2O_7$ ultrafine powders." Ceramics International **42.5** (2016): 6221–6227.

36. Huang, Zhaoxiang, Buyin Li, and Jia Liu. "Molten-salt synthesis of oxyapatite $La_{9.33}Si_6O_{26}$ powders as electrolytes for intermediate temperature solid oxide fuel cells." physica status solidi (a) **207.10** (2010): 2247–2251.

37. Vradman, Leonid, et al. "Synthesis of $LaMnO_3$ in molten chlorides: effect of preparation conditions." Physical Chemistry Chemical Physics **15.26** (2013): 10914–10920.

38. Sangster, James, and Arthur D. Pelton. "Phase diagrams and thermodynamic properties of the 70 binary alkali halide systems having common ions." Journal of Physical and Chemical Reference Data **16.3** (1987): 509–561.

39. Basin, A. S., et al. "The LiCl-KCl binary system." Russian Journal of Inorganic Chemistry **53.9** (2008): 1509–1511.

40. Cho, Yong-Jun, et al. "Characteristics of oxidation reaction of rare-earth chlorides for precipitation in LiCl-KCl molten salt by oxygen sparging." Journal of Nuclear Science and Technology **43.10** (2006): 1280–1286.

41. Lee, Seungho, et al. "LSCF–SDC core–shell high-performance durable composite cathode." Journal of Power Sources **195.1** (2010): 118–123.

42. Gang, L. I. U., et al. "Synthesis of α-Fe_2O_3@ SnO_2 core-shell nanoparticles via low-temperature molten salt reaction route." Transactions of Nonferrous Metals Society of China **25.11** (2015): 3651–3656.

43. Tian, Xuelin, et al. "Template-free and scalable synthesis of core−shell and hollow $BaTiO_3$ particles: using molten hydrated salt as a solvent." Crystal Growth & Design **9.11** (2009): 4927–4932.

44. Alaparthi, Suresh Babu. Synthesis and luminescence properties of core-shell structured (lanthanum (1-x) europium (x)) (2) zirconium heptoxid [at] yttrium orthoborate spherical nanoparticles. M.S. Thesis, The University of Texas-Pan American, 2012.

45. Zhao, Wei, et al. "Sacrificial template synthesis of core-shell $SrTiO_3$/TiO_2 heterostructured microspheres photocatalyst." Ceramics International **43.6** (2017): 4807–4813.

46. Wang, Qian, et al. "Core/shell structured La-and Rh-codoped $SrTiO_3$ as a hydrogen evolution photocatalyst in Z-scheme overall water splitting under visible light irradiation." Chemistry of Materials **26.14** (2014): 4144–4150.

47. Takeuchi, Tsuguto, Toshihiko Tani, and Toshikazu Satoh. "Microcomposite particles $Sr_3Ti_2O_7$–$SrTiO_3$ with an epitaxial core–shell structure." Solid State Ionics **108.1** (1998): 67–71.

48. Lauhon, Lincoln J., et al. "Epitaxial core-shell and core-multishell nanowire heterostructures." Nature **420.6911** (2002): 57.

49. Li, Binbin, et al. "Core–shell $SrTiO_3$: $Yb^{3+,}$ Er^{3+}@ $mSiO_2$ nanoparticles for controlled and monitored doxorubicin delivery." RSC Advances **6.31** (2016): 26280–26287.

50. Choi, Ju H., et al. "Synthesis of core-shell Y_2O_3 nanoparticles for enhanced luminescence efficiency." Active Photonic Materials V. Proceedings of SPIE **8808** (2013): 88081N.

51. Joo, Sang Hoon, et al. "Thermally stable Pt/mesoporous silica core-shell nanocatalysts for high-temperature reactions." Nature Materials **8.2** (2009): 126.

52. Porter, David A., Kenneth E. Easterling, and Mohamed Sherif. Phase Transformations in Metals and Alloys, (Revised Reprint). CRC Press, 2009.

53. Liu, X. Y. "Heterogeneous nucleation or homogeneous nucleation?" The Journal of Chemical Physics **112.22** (2000): 9949–9955.

54. Dubrovskii, Vladimir. "Fundamentals of Nucleation Theory." Nucleation Theory and Growth of Nanostructures. Springer Berlin Heidelberg, 2014. 1–73.

55. Gránásy, László, et al. "Heterogeneous nucleation of/on nanoparticles: a density functional study using the phase-field crystal model." Chemical Society Reviews **43.7** (2014): 2159–2173.

56. Morales, L., et al. "Structural and magnetotransport properties of $LaMn_{1-x}Cr_xO_{3.00}$ ($0 \leqslant x \leqslant 0.15$): Evidence of Mn^{3+}–O–Cr^{3+} double-exchange interaction." Physical Review B **72.13** (2005): 132413.

57. Yang, Zhongqin, Ling Ye, and Xide Xie. "Density-functional studies of magnetic and electronic structures for the perovskite oxides $LaMn_{1-x}Cr_xO_3$." Journal of Physics: Condensed Matter **12.12** (2000): 2737.

58. Deisenhofer, Joachim, et al. "Interplay of superexchange and orbital degeneracy in Cr-doped $LaMnO_3$." Physical Review B **66.5** (2002): 054414.

59. Zhang, L. W., et al. "The magnetotransport properties of $LaMn_{1-x}Cr_xO_3$ manganites." Journal of Magnetism and Magnetic Materials **219.2** (2000): 236–240.

60. Gerlach, Gerald, and Wolfram Dotzel. Introduction to microsystem technology: a guide for students. John Wiley & Sons, 2008.

61. Miyoshi, Shogo, and Manfred Martin. "B-Site cation diffusivity of Mn and Cr in perovskite-type $LaMnO_3$ with cation-deficit nonstoichiometry." Physical Chemistry Chemical Physics **11.17** (2009): 3063–3070.

CURRICULUM VITAE